



# The Effect of Annealing on the Properties of AW5754 Aluminum Alloy-AZ31B Magnesium Alloy Explosively Welded Bimetals

Miroslav Sahul, Martin Sahul, Ján Lokaj, Ľubomír Čaplovič, Petr Nesvadba, and Barbara Odokienová

(Submitted January 10, 2019; in revised form August 17, 2019; published online October 3, 2019)

Explosive welding of AW5754 aluminum alloy to AZ31B magnesium alloy was performed. AW5754 was proposed as a flyer plate. A parallel setup was used during explosive welding. The annealing of AW5754/AZ31B composite plate at 250, 300 and 350 °C for 2, 3, 4 and 5 h was performed after explosive welding. Bimetals were characterized by regular wavy interface. Annealing resulted in the creation of intermetallic compounds (IMCs). The increase in the thickness of IMC interfacial layer was observed with increasing of annealing temperature and time. IMC layer of highest thickness was recorded after annealing at 350 °C for 5 h and averaged 67 μm. EDS analysis showed that the interfacial layer close to AW5754 alloy was formed by Al<sub>3</sub>Mg<sub>2</sub> IMC, and interfacial layer adjacent to the AZ31B alloy consisted of Mg<sub>17</sub>Al<sub>12</sub> IMC. Bright particles were spread at the AW5754-Al<sub>3</sub>Mg<sub>2</sub> IMC interface. Rise in the microhardness at the interface of produced bimetal was associated with work hardening. Microhardness values increased to 218 HV0.025 after annealing process due to IMCs present at the interface. Decrease in microhardness in locations close to the IMC interfacial layer was found after heat treatment due to recrystallization. The bimetal tensile strength reached 120 MPa. The annealing resulted in decrease in the bimetal tensile strength.

**Keywords** aluminum alloy, annealing, detonation velocity, explosive welding, intermetallic compounds, magnesium alloy

## 1. Introduction

The weight reduction in vehicles belongs to the major endeavors for reducing the production costs, fuel consumption and thus environmental impact in automotive industry (Ref 1-6). Magnesium and its alloys have been studied due to their high strength-to-weight ratio, low density and high damping capacity (Ref 7, 8). Contrary, the lower corrosion resistance and ductility at room temperature associated with hexagonal close-packed structure are the main roots that limit the more extensive utilization of magnesium and its alloys (Ref 9, 10). The problem with poor resistance to corrosion of magnesium alloys can be solved by various techniques, such as deposition of Al coating (Ref 11-14) or manufacturing of Al/Mg composite

structures (Ref 4, 5, 8, 9, 15-18). Thus, magnesium and aluminum alloys manufactured as composite structures can enhance the resistance to corrosion and take the advantage of mentioned light alloys (Ref 18-21). In the past decades, aluminum and magnesium alloys have been joined by conventional fusion and solid-state welding, as gas tungsten arc welding (GTAW) (Ref 15, 22), laser (Ref 10, 23) and laser welded bonding (LBW) (Ref 24), cold metal transfer welding (CMT) (Ref 25-27), resistance spot welding (Ref 28, 29), brazing (Ref 30, 31), diffusion bonding (Ref 32-37), friction stir welding (FSW) (Ref 1, 15, 38-42), ultrasonic spot welding (Ref 43), magnetic pulse welding (MPW) (Ref 5) and explosion welding (Ref 8, 9, 18, 44). However, mainly fusion welding methods are not suitable to metallurgically join aluminum alloys to magnesium alloys. Conventional fusion welding methods produce weld metal which contains large number of IMCs leading to formation of cracks considerably influencing the strength of weld joint. Many issues in fusion welding of mentioned light alloys could be encountered, as cracking, oxide impurities and creation of hard and brittle IMCs. Thus, the attention is focused on joining dissimilar light alloys via solid-state welding technologies like explosive welding. The main characteristic of explosive welding is the utilization of high kinetic energy of flyer plate being accelerated by detonation wave spreading along the base metal. The distance between base metal and flyer plate is called stand-off distance. Jet is created during explosive welding and is responsible for removing surface oxides and thus for production of sound solid-state bond (Ref 45). The research dealing with welding of aluminum to magnesium by explosive welding and further annealing is underway worldwide. Chen et al. investigated the microstructural characteristics and mechanical properties of multi-pass rolled and annealed aluminum-magnesium bimetals. The authors found that the increase in temperature and holding time resulted firstly in the rise in the mechanical properties of

**Miroslav Sahul**, Department of Welding and Joining of Materials, Faculty of Materials Science and Technology in Trnava, Institute of Production Technologies, Slovak University of Technology in Bratislava, J. Bottu 25, 917 24 Trnava, Slovak Republic; **Martin Sahul**, **Ján Lokaj**, **Ľubomír Čaplovič**, and **Barbara Odokienová**, Faculty of Materials Science and Technology in Trnava, Institute of Materials Science, Slovak University of Technology in Bratislava, J. Bottu 25, 917 24 Trnava, Slovak Republic; **Petr Nesvadba**, OZM Research, s.r.o., Blížňovce 32, 538 62 Hrochův Týnec, Czech Republic. Contact e-mails: miroslav.sahul@stuba.sk, martin.sahul@stuba.sk, jan.lokaj@stuba.sk, lubomir.caplovic@stuba.sk, nesvadba@ozm.cz, and barbara.odokienkova@stuba.sk.

welds and in decrease in values when annealing temperature reached 300 °C. Furthermore, mixed mode fractures were observed on fracture surfaces (Ref 46). Fronczek et al. observed in their A1050/AZ31/A1050 trimetals produced by explosion welding equiaxed and columnar-grained  $Mg_2Al_3$  compound and columnar-grained  $Mg_{17}Al_{12}$  compound. Moreover, authors found also traces of  $Mg_{23}Al_{30}$  IMC (Ref 9). Similarly, Zhang et al. observed creation of interfacial layer consisting of  $Al_3Mg_2$  and  $Al_{12}Mg_{17}$  after annealing at the temperature of 250 °C and higher. They also noticed the delamination of bimetals after annealing at the temperature of 250 °C and higher (Ref 18). Zhang et al. studied microstructure and mechanical properties of AA6061/AZ31B explosively welded bimetal. Authors found that adiabatic shear bands (ASBs) were formed in directions of concentration of stress waves. Crystallized grains were observed in AZ31B magnesium alloy, and elongated ones were found in AA6061 aluminum alloy flyer (Ref 47). Ding et al. analyzed the influence of the annealing on the properties of diffusion welded aluminum and magnesium alloys. They observed that the thickness of interface layers increased as the annealing temperature increased, and the minimum residual stresses and highest tensile strength were observed after annealing at 250 °C. Therefore, the authors recommended the temperature of 250 °C as the most suitable for annealing of diffusion welds (Ref 48).

Luo et al. fabricated 5052/AZ31/5052 alloy laminated composite plates using two-pass hot-rolling process. They observed that annealing at 300 °C or higher resulted in the creation of continuous interfacial layers of  $Mg_{17}Al_{12}$  and  $Al_3Mg_2$  compounds. IMC layer was broken after second rolling pass and its fractions were observed at the interface zone (Ref 49). Macwan et al. investigated the influence of annealing on the microstructure and mechanical properties of Al/Mg/Al trimetals produced by rolling. The authors found that annealing at 250 °C and below mentioned temperature was characterized by the absence of interface debonding during the tensile testing. On the contrary, partial debonding occurred through cracking at the location of IMCs after annealing at 300 °C or higher (Ref 50).

Zhang et al. prepared 7075/AZ31B/7075 composites through roll bonding. The authors found that the increase in reduction ratio and rolling temperature led in drop of strength resulting from grain coarsening and thickening of the IMC layer. The highest strength of the composite plate reached 66 MPa (Ref 20).

Nevertheless, there is limited amount of research papers focusing on the explosive welding and subsequent annealing of the combination of AW5754 aluminum alloy with the magnesium as main alloying element and AZ31B magnesium alloy. On that account, the present study deals with the influence of the annealing process on the properties of produced AW5754 aluminum alloy-AZ31B magnesium alloy bimetal produced by explosive welding.

## 2. Experimental

### 2.1 Welded Materials and Welding Setup Specification

1.5-mm-thick AW5754 aluminum alloy and 14-mm-thick AZ31B-H24 (half hard) magnesium alloy were suggested as experimental materials for explosive welding. AW5754 alu-

minum alloy was designed as the flyer sheet, and magnesium alloy was proposed as the base material due to lower plasticity resulting from hexagonal close-packed (hcp) crystal structure. The chemical composition of AW5754 aluminum alloy flyer sheet (in wt.%) is Mg (2.6-3.6), Mn ( $\leq 0.5$ ), Fe ( $\leq 0.4$ ), Si ( $\leq 0.4$ ), Cr ( $\leq 0.3$ ), Zn ( $\leq 0.2$ ), Ti ( $\leq 0.15$ ), Cu ( $\leq 0.1$ ) and Al (balance), and that of AZ31 magnesium alloy base material (in wt.%) is Al (2.5-3.5), Zn (0.7-1.3), Mn (0.2), Si ( $\leq 0.05$ ), Cu ( $\leq 0.05$ ), Ca ( $\leq 0.04$ ), Fe ( $\leq 0.005$ ), Ni ( $\leq 0.005$ ) and Mg (balance).

AW5754 flyer sheet width and length were 130 and 180 mm, respectively. The size of AZ31B-H24 base material was 90 × 137 mm. The dimensions of flyer plate were proposed to be larger due to mounting wooden frame for the explosive. Inner dimensions of the wooden frame were as follows: 115 × 179 × 12.8 mm. From the mentioned dimensions, it follows that the explosive thickness is 12.8 mm.

The explosive thickness  $t_e$  in the case of welding using the Semtex S type explosives equals approximately to flyer sheet thickness  $t_f$  multiplying by 10, i.e.,  $t_e \approx 10 \cdot t_f$ . Given relationship could be applied for the flyer sheet thicknesses ranging from 1 to 4 mm. The general scheme of the explosive welding process is given in Fig. 1. Parallel setup of materials was used to produce lightweight bimetal. The bimetal was produced in collaboration with OZM Research, s.r.o. company in Hrochův Týnec, Czech Republic.

Parallel arrangement of materials was used for explosive welding. As it is known, detonation velocity is the same as collision point velocity. Stand-off distance of 3.0 mm between welded materials was adjusted by wooden pins. Semtex S30 loose explosive was used for welding of light alloys. Detonation velocity of explosive was determined by measurement of the time during which the detonation front propagates between points 1 and 2 (Fig. 2a). Yokogawa TC120 multifunctional universal counter was used for time measurement. In order to activate the loose explosive, Starline<sup>®</sup> 12 detonating cord was applied. Detonation velocity of Starline<sup>®</sup> 12 was 6500 m/s. The explosively weld joints were fabricated in order to produce transition joints for the cryogenics. The next application could be in the area of the production of light ballistic materials. The huge potential is especially in the production of composite materials for aerospace industry. The need for annealing process results from the higher deformations and residual stresses originating during explosive welding process. So, in the next step, the flattening of bent composite by press at higher temperature is of great importance. Contrary, the temperature is

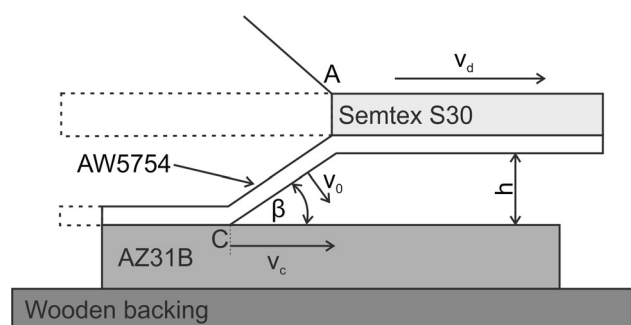


**Fig. 1** Schematic overview of explosive welding process,  $\beta$ —dynamic angle of collision,  $v_d$ —detonation velocity of explosive,  $v_0$ —flyer sheet velocity,  $h$ —stand-off distance,  $v_c$ —collision point velocity, C—collision point, A—detonation front

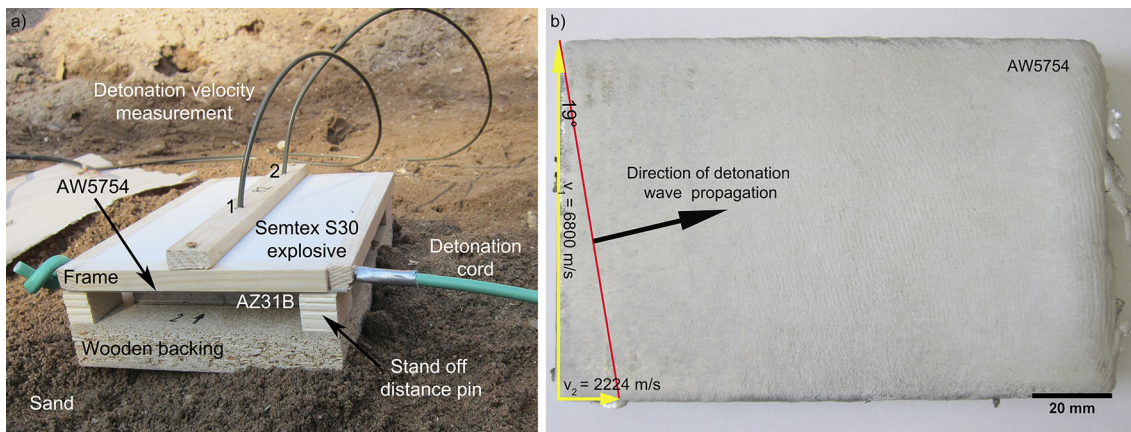


**Fig. 2** (a) Parallel setup before explosive welding; (b) produced AW5754-AZ31B bimetal

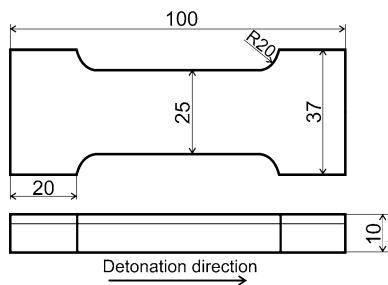


**Fig. 3** Dimensions of tensile testing specimen (in mm)

the driving force for diffusion process. From this point of view, it is necessary to study the effect of heat treatment on the interface properties.

Detonation velocity of Semtex S30 was 2224 m/s. The weight and density of used loose explosive were 263.1 g and 1.0 g/cm<sup>3</sup>, respectively. Firstly, the flyer sheet with the mounted wooden frame and detonating cord were weighed. In the next step, the frame was filled with the loose explosive and weighed. Explosive weight was then calculated as the difference between mentioned weights.

AW5754-AZ31B composite plate after explosive welding is documented in Fig. 2b. The direction of propagation of detonation wave is marked by an arrow. Based on known detonation velocity of Starline 12 detonation cord and measured detonation velocity of Semtex loose explosive, the propagation of detonation wave was estimated. The macrostructures were cutoff from the center part bimetal in the welding direction (i.e., direction of the propagation of detonation wave). First stage of metallographic preparation of as-welded and as-annealed samples consisted of grinding with P1200 emery paper. PoliCloth and TriDent polishing cloths were used for polishing with 9 and 3 μm diamond suspensions. Buehler VibroMet™ 2 was used for vibration polishing of samples. Vibration polishing time was 20 min.

## 2.2 Annealing of Bimetals

The annealing of composite plates at 250, 300 and 350 °C for 2, 3, 4 and 5 h was performed after welding. LMV muffle vertical furnace with air atmosphere from LAC Company was used for annealing process. The heating rate was 30 °C/min. The annealing temperature of the bimetals was controlled using

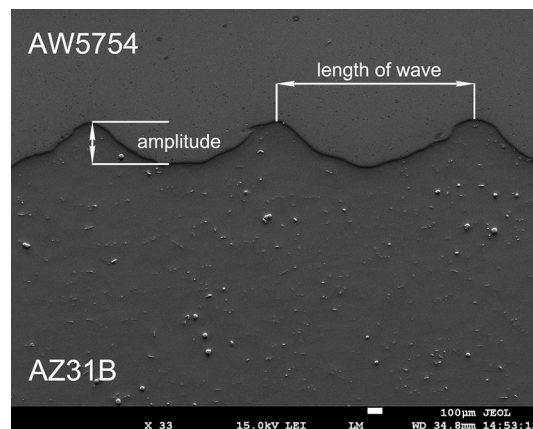


**Fig. 4** Wavy interface of bimetal after explosive welding

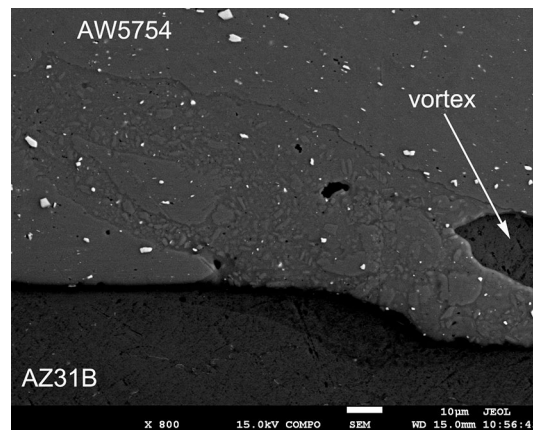


**Fig. 5** Vortex present at the bimetal interface

thermocouple. The bimetals were taken out of the furnace after passing the annealing time, and the following cooling took place in the air.

## 2.3 Analytical Methods

Analysis of the thicknesses of IMCs present at the composite plate interface, elemental line scans and mappings,

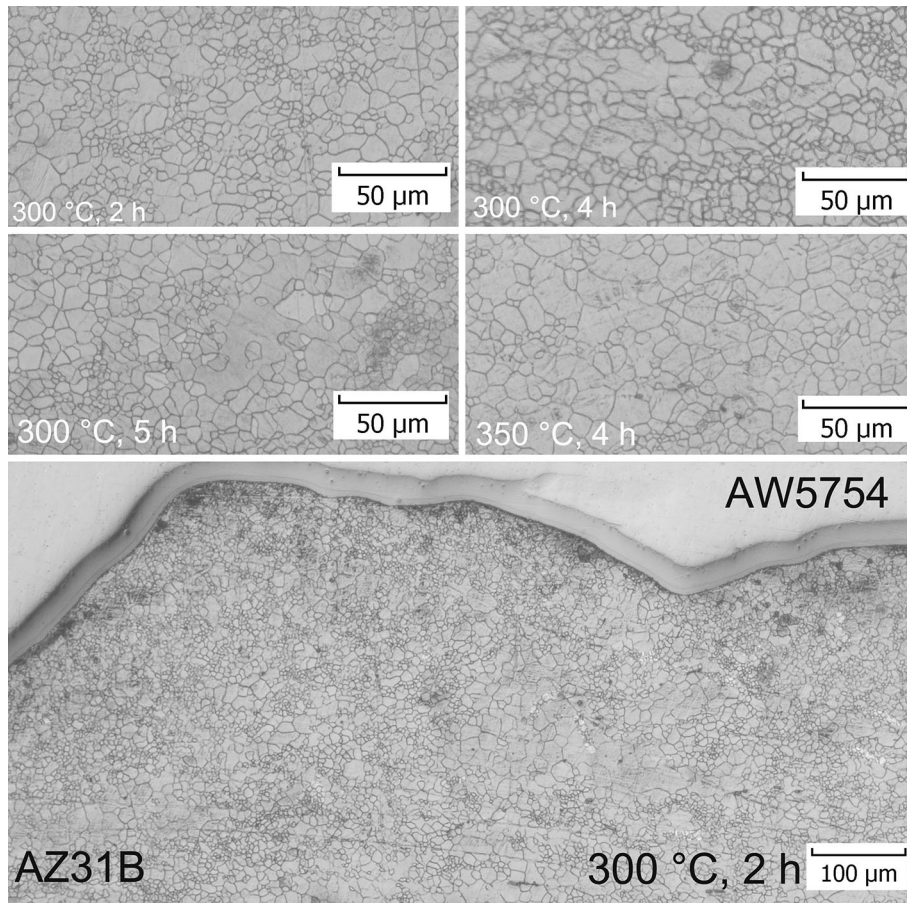


**Fig. 6** Microstructure of bimetal after annealing at different heat treatment regimes

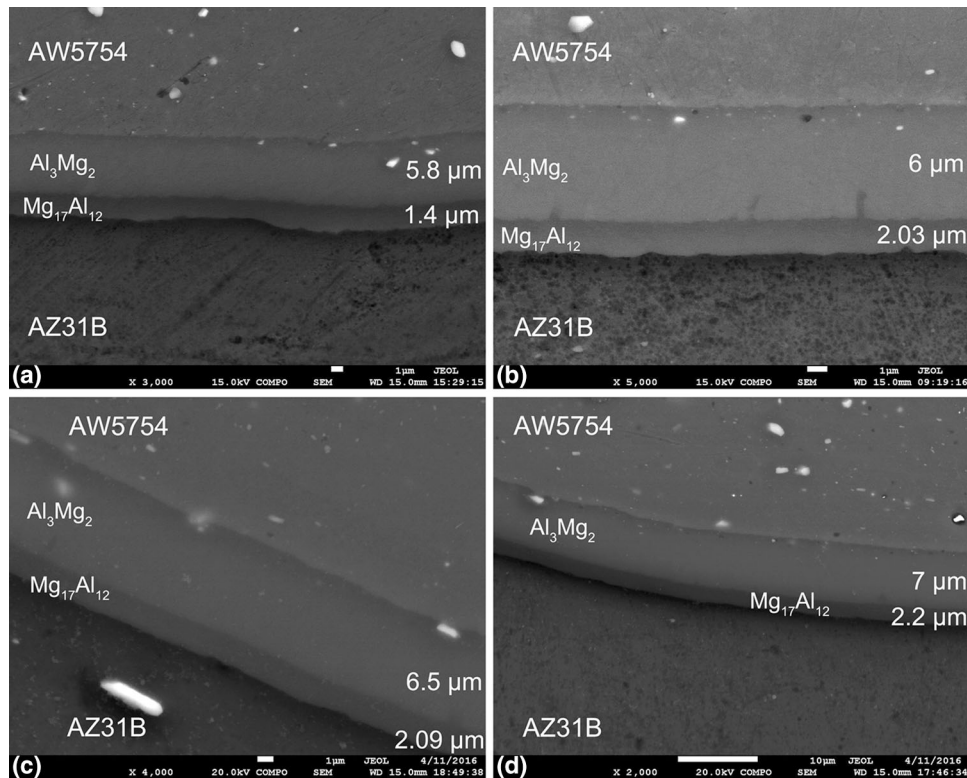


**Fig. 7** Interface after annealing at 250 °C for annealing times of (a) 2; (b) 3; (c) 4 and (d) 5 h

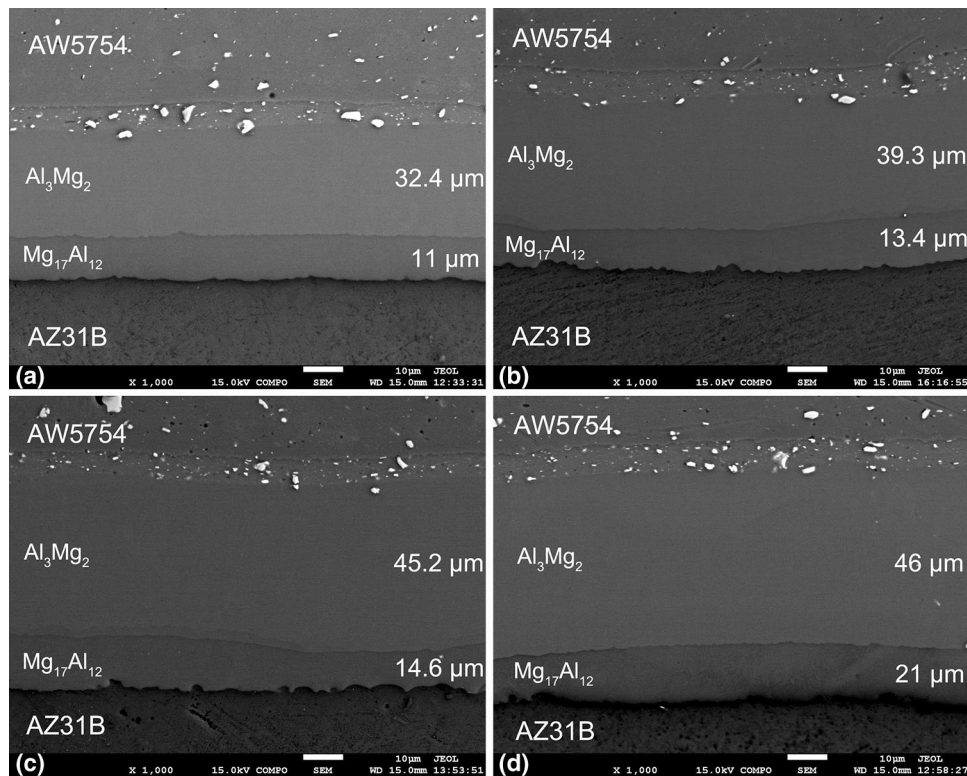


**Fig. 8** Interface after annealing at 350 °C for annealing times of (a) 2; (b) 3; (c) 4 and (d) 5 h

local chemical composition and fracture surfaces after tensile testing as well as was carried out with the use of JEOL JSM 7600 field-emission gun electron microscope. X-max 50 mm<sup>2</sup> (large area silicon drift detector) of Oxford Instruments was used for EDS analysis.

Qualitative XRD analysis with the use of Empyrean diffractometer with PIXcel<sup>3D</sup> detector (Cu anode,  $\lambda_{\text{CuK}\alpha} = 0.1541874$  nm) was used to characterize the IMCs formed at the interface after annealing of bimetals. The parameters for measurement were as follows:  $U = 40$  kV,  $I = 40$  mA, step size  $0.02^\circ 2\Theta$  and interval  $30^\circ\text{--}110^\circ 2\Theta$ .

Buehler IndentaMet 1100 microhardness tester was utilized for measurement of microhardness through AW5754 aluminum alloy-AZ31B magnesium alloy interface. Loading force was 245.25 mN and dwell time 10 s.

Room temperature tensile properties of the bimetals were determined with the Tinius Olsen Model 300 ST electromechanical universal testing machine (max. load force 300 kN). The crosshead speed was 5 mm/s. The specimens for tensile testing were machined according to EN ISO 4136, oriented along the detonation direction, and loading of the bimetal during tensile testing was along welding direction. The dimensions of tensile test specimens (in mm) are given in Fig. 3.

### 3. Results

#### 3.1 Microstructure Analysis of Bimetals

AW5754 aluminum alloy-AZ31 magnesium alloy bimetal interface is documented in Fig. 4. The interface was regular and wavy confirming the typical feature for explosive welding.

Variation of the jet flow result from the behavior of metals during explosive welding is the cause of formation of wavy interface. It is supposed that materials behave like fluids under the condition of acting high pressures and high rates of deformation. The jet enables removal of surface oxides, resulting in a good metallurgical bonding (Ref 8). Metallographic observations showed that the collision between welded materials was homogeneous, resulting in formation of regular interface (Ref 51).

No continuous IMC layer was found at the as-welded bimetal interface. In some locations, zones with IMC were observed, but these had not significant influence on the overall mechanical properties of produced bimetals. Based on EDS analysis results (see chapter 3.4.1),  $\text{Mg}_{17}\text{Al}_{12}$  IMC could be present in that locations. Chen et al. observed the interfacial layer after magnetic pulse welding of mentioned materials. The average thickness of layer was 26  $\mu\text{m}$  when 5 kV discharge voltage was used. They observed decrease in interfacial layer thickness to 3.5 and 2.1  $\mu\text{m}$  after decreasing discharge voltage to 4.5 and 4 kV (Ref 5). Contrary, the thickness of IMC present at the interface in our case was lower, only about 1.45  $\mu\text{m}$ .

Microscopic observations in our case confirmed the soundness of the as-welded interface. Furthermore, no voids and delamination were observed (Ref 52-54).

The average length of waves was  $1218 \pm 48$   $\mu\text{m}$ , and amplitude of waves was  $276 \pm 11$   $\mu\text{m}$ . Similarly, Fronczek et al. (Ref 9) found in their A1050/AZ31/A1050 explosion welded trimetal wavy morphology character of interfaces with the amplitude of waves up to 300  $\mu\text{m}$ .

Carvalho et al. observed that the explosion welds between aluminum alloys (6082-0 flyer and 6082-T6 base metal) showed wavy morphology irrespective of the mechanical properties of the different flyer sheets used for joining. Some

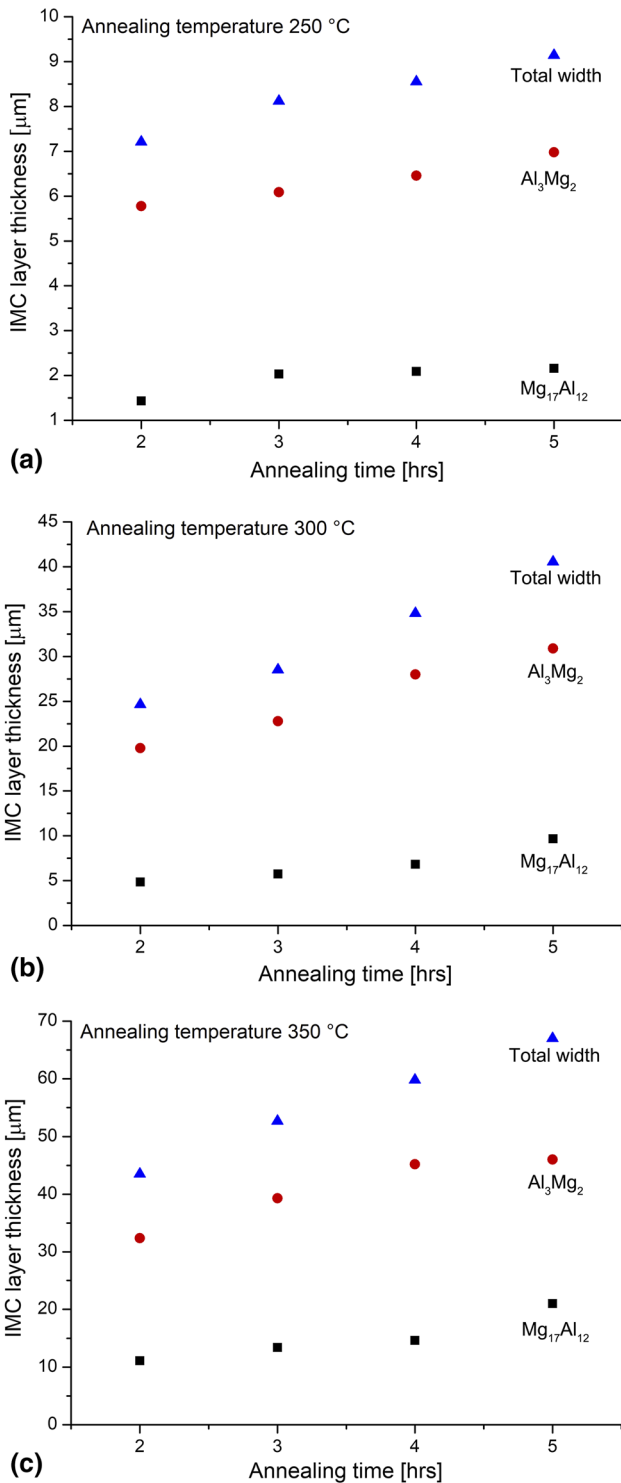


**Fig. 9** Dependence of annealing time on the IMC layer thickness for annealing temperature (a) 250 °C; (b) 300 °C; (c) 350 °C

melted areas were observed at the upper and lower zones of the waves (Ref 55). Similarly, wavy interface was observed also by Greenberg et al. in explosive welded copper-tantalum bimetals and silver-iron welds as well (Ref 56). Lazurenko et al. observed in their titanium-aluminum explosively welded sandwich the evident influence of the distance from the explosive on the morphology of individual interfaces. Clearer wave morphology was observed at the distances nearer to the explosive

**Table 1** Values of growth rate constant  $k$  for  $\text{Mg}_{17}\text{Al}_{12}$  and  $\text{Mg}_2\text{Al}_3$  IMCs at the annealing temperatures of 250, 300 and 350 °C

Annealing temperature, °C	Growth rate constant $k$ , $\text{m}^2/\text{s}$ for $\text{Mg}_{17}\text{Al}_{12}$	Growth rate constant $k$ , $\text{m}^2/\text{s}$ for $\text{Mg}_2\text{Al}_3$
250	$2.25 \times 10^{-16}$	$1.4 \times 10^{-15}$
300	$6.19 \times 10^{-15}$	$5.42 \times 10^{-14}$
350	$2.74 \times 10^{-14}$	$1.03 \times 10^{-13}$

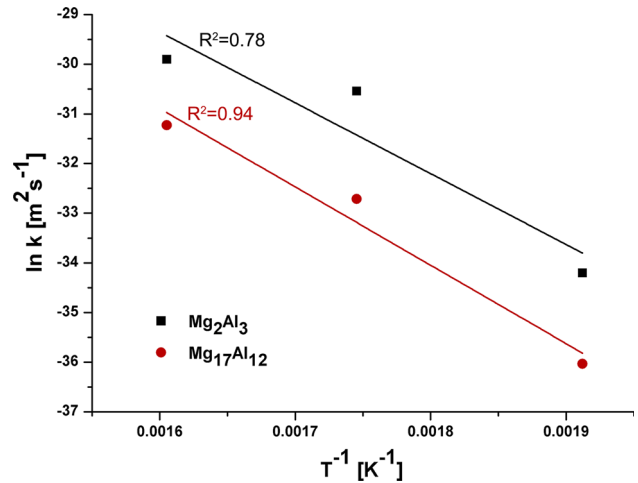


**Fig. 10** Dependence of  $\ln k$  on  $1/T$  for  $\text{Mg}_{17}\text{Al}_{12}$  and  $\text{Al}_3\text{Mg}_2$  IMCs

position. The interfaces between lower sheets being most distant from the explosive were almost flat (Ref 57). Thermal cycles acting during explosive welding are very short. The materials to be welded undergo very fast heating as a result of high strain rate. Thus, melting and intermixing of metals occurred, leading to the formation of so-called vortices (Ref 58). Mentioned vortices (Fig. 5) were observed at some locations at the Al-Mg bimetal interface. Vortices are formed due to intermixing of welded metals at high temperature followed by rapid cooling during explosive welding (Ref 57).

Microstructures of AZ31B part of bimetal after various regimes of annealing are given in Fig. 6. It was observed that recrystallization occurred during annealing process. The average grain size in the distance at 100  $\mu\text{m}$  was 6  $\mu\text{m}$  for bimetal after annealing at 300 °C for 2 h. Zone of very fine grains was observed in this case.

Locations where number of dislocations increases, i.e., near grain or twin boundaries, are potential sites for nucleation of new grains. It was observed that work hardening occurred during explosive welding process. Thus, the areas close to the interface exhibited severe plastic deformation. Generally, the higher the degree of deformation the lower temperature is needed for recrystallization. At the distance of about 229  $\mu\text{m}$ , larger grains were observed. The average grain size was in this location 11.8  $\mu\text{m}$ . Similar situation was recorded after annealing at the same temperature but for 4 h. Locations with very fine grains alternated with zones containing larger ones. The average grain size was 5.2  $\mu\text{m}$ . The reason was that during longer period more grains nucleated at the original grain

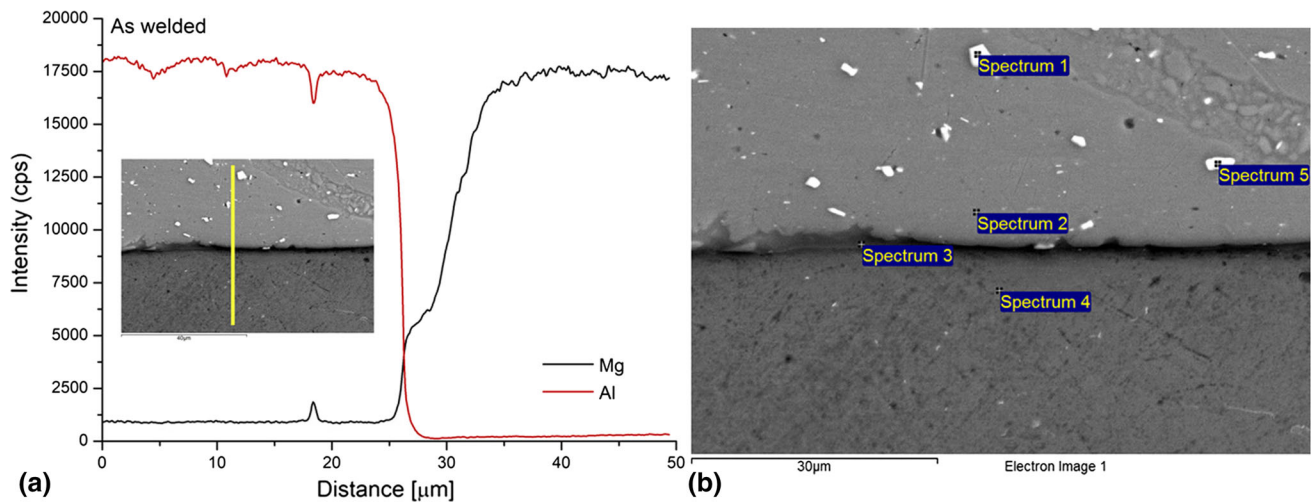


**Fig. 11** (a) Elemental line scans of Al and Mg across as-welded bimetal interface, (b) point EDS analysis at the as-welded bimetal interface

boundaries. When annealing time 5 h was used, grain coarsening was observed. The average grain size was 7.5 μm in such a case. Finally, the influence of temperature was more evident. When the temperature increased to 350 °C (time was 5 h as in the previous case), the grain size increased to 11.2 μm. Here, the higher temperature resulted in grain coarsening.

### 3.2 SEM Analysis of the Bimetal Interfaces after Annealing Process

SEM images of bimetal interface after annealing at 250 °C for 2, 3, 4 and 5 h are given in Fig. 7(a), (b), (c), and (d). Intermetallic compound layer was observed after annealing. It was found that the thickness of the IMC layer increases with increasing the annealing time. The mentioned layer consisted of two sub-layers, corresponding to  $\text{Al}_3\text{Mg}_2$  and  $\text{Mg}_{17}\text{Al}_{12}$  IMC. As it follows from SEM images,  $\text{Al}_3\text{Mg}_2$  is thicker in comparison to  $\text{Mg}_{17}\text{Al}_{12}$ .

As it is known, the diffusion coefficient in solid materials is dependent on the annealing temperature. Generally, the higher the annealing temperature the thicker the intermetallic layer (Ref 18). SEM images of bimetal interface after annealing at 350 °C for annealing times 2, 3, 4 and 5 h are given in Fig. 8(a), (b), (c), and (d). The bright particles were accommodated in that location because of the low solubility of iron in aluminum at the annealing temperatures used (Ref 50).

The dependences of annealing time on the IMC layer thickness for annealing temperatures of 250, 300 and 350 °C are given in Fig. 9(a), (b), and (c). The temperature of annealing was 250 °C in this case (Fig. 7a). The IMC layer consisted of two layers. The thickness of  $\text{Mg}_{17}\text{Al}_{12}$  IMC was lower in comparison to  $\text{Al}_3\text{Mg}_2$ .  $\text{Mg}_{17}\text{Al}_{12}$  thickness after 2 h of annealing at 250 °C averaged 1.4 μm. The mentioned IMC thickness increased with the increase in annealing time. The maximum thickness from the tested parameters of annealing was in this case observed after 5 h. The  $\text{Mg}_{17}\text{Al}_{12}$  thickness was 2.2 μm and for  $\text{Al}_3\text{Mg}_2$  6.9 μm. The overall thickness of IMC present at the interface was 9.1 μm.

The dependence of annealing time on the IMC layer thickness is shown in Fig. 7(b), and annealing temperature was 300 °C. The application of higher annealing temperature led to increasing of overall thickness of IMC. The maximum thickness was similarly measured after annealing for 5 h. The

**Table 2** EDS linescan and point analysis of the as-welded bimetal interface (in at.%)

Spectrum	Mg	Al	Si	Cr	Mn	Fe	Zn
1	1.50	82.23	3.18	0.32	2.74	10.03	...
2	7.81	89.40	2.71	...	0.08	...	...
3	66.72	32.17	0.06	...	0.10	...	0.96
4	96.75	2.33	0.11	...	0.15	...	0.66
5	4.63	79.80	3.34	0.31	4.63	7.31	...

$\text{Mg}_{17}\text{Al}_{12}$  thickness was 9.7 μm and for  $\text{Al}_3\text{Mg}_2$  31 μm. The overall thickness of IMC present at the interface was 40.7 μm.

The dependence of annealing time on the IMC layer thickness at temperature of 350 °C is shown in Fig. 7(c). The higher annealing temperature resulted similarly in increasing of the thickness of IMC. The  $\text{Mg}_{17}\text{Al}_{12}$  maximum thickness was 21 μm and for  $\text{Al}_3\text{Mg}_2$  46 μm. The overall thickness of IMC present at the interface was 67 μm.

### 3.3 Kinetics of IMCs Interfacial Sub-layers Growth

The dependence of the IMC thickness on annealing time can be characterized by following equation:  $Y^n = k \cdot t$ , where  $Y$  is the thickness of IMC,  $k$  is the growth rate constant,  $t$  is the annealing time, and  $n$  is the growth rate time constant. The growth rate constant can be obtained after the construction of the dependence of IMC layer thickness  $Y^2$  (m<sup>2</sup>) versus annealing time  $t$  (s). The growth rate constants  $k$  for  $\text{Mg}_{17}\text{Al}_{12}$  and  $\text{Mg}_2\text{Al}_3$  IMCs are given in Table 1. The growth rate constant at given annealing temperature is higher for  $\text{Mg}_2\text{Al}_3$  IMC. As it follows from Arrhenius equation, the growth rate constant is a function of reciprocal value of annealing temperature:  $k = k_0 \exp\left(-\frac{Q}{RT}\right)$ , where  $k_0$  is the pre-exponential factor (m<sup>2</sup>/s),  $Q$  is activation energy (J/mol),  $R$  is the universal gas constant 8.314 (J/(mol K)), and  $T$  is the absolute annealing temperature (K) (Ref 59, 60).

Activation energy of IMC can be expressed by logarithm relationship with the growth rate constant. Dependence of  $\ln k$  versus  $\frac{1}{T}$  for  $\text{Mg}_{17}\text{Al}_{12}$  and  $\text{Mg}_2\text{Al}_3$  IMC is shown in Fig. 10. Activation energy  $Q$  and pre-exponential factor  $k_0$  were then calculated. Activation energy for  $\text{Mg}_{17}\text{Al}_{12}$  IMC growth is

131.2 kJ/mol and for  $Mg_2Al_3$  IMC growth is 118.5 kJ/mol. Lower activation energy is needed for growing of  $Mg_2Al_3$  resulting in higher thickness of mentioned IMC in comparison to  $Mg_{17}Al_{12}$ .

Macwan et al. mentioned in their study that activation energy for  $Mg_{17}Al_{12}$  IMC growth was  $165 \pm 6$  kJ/mol and 85.5 kJ/mol for  $Mg_2Al_3$ . But the authors analyzed the properties of trimetal clads consisting of the pure aluminum A1060 and Mg-0.2Al-1.75Mn-0.75Ce alloy (Ref 50). In our study, the presence of alloying elements in the AW5754 aluminum alloy could increase the activation energy for  $Mg_2Al_3$  IMC. Li et al. calculated activation energy  $Q$  for  $Mg_{17}Al_{12}$  to be  $106.2 \pm 3.1$  kJ/mol and for  $Mg_2Al_3$   $57.1 \pm 1.5$  kJ/mol. The authors similarly used pure aluminum plate (99.99%) in their study (Ref 61).

### 3.4 EDS Analysis

**3.4.1 EDS Analysis of As-welded Bimetal.** Aluminum and magnesium elemental “linescans” across AW5754 aluminum alloy-AZ31B magnesium alloy bimetal interface (across yellow line) in as-welded condition are shown in Fig. 11(a).

It is evident that concentration of magnesium increases toward bimetal interface and AZ31B-H24 magnesium alloy base material. No continuous IMC layer was observed after explosive welding. In some locations, very narrow gray areas

probably of IMC were observed. Thus, point EDS analysis was carried out at the as-welded bimetal interface (Fig. 11b). Local zone of IMC was very thin. The measured thickness reached the value only of 1.45  $\mu m$ .

Results of point EDS analysis are given in Table 2. The chemical composition of the interfacial area corresponds to the Spectrum 3. The content of magnesium is about 66.7, and 32.2 at.% of aluminum was measured here. Alloying elements Zn, Mn and Si were also detected. This indicates that  $Mg_{17}Al_{12}$  IMC could be present in this location after welding process. The formation of local zones of IMC at the interface during explosive welding is associated with very high pressures acting during welding on the interface. In this case, high pressure causes heating of material to high temperatures for very short time in explosive welding.

**3.4.2 EDS Analysis of As-annealed Bimetals.** Aluminum and magnesium elemental “linescans” across AW5754 aluminum alloy-AZ31B magnesium alloy bimetal interface (yellow lines in Fig. 12 and 13) after annealing at 250 and 350  $^{\circ}C$  for 2, 3, 4 and 5 h are shown in Fig. 12 and 13. It was found that the concentration of magnesium decreased from AZ31B alloy side toward AW5754 aluminum alloy. On the other hand, the drop of aluminum concentration was observed from AW5754 aluminum alloy toward magnesium alloy. Two

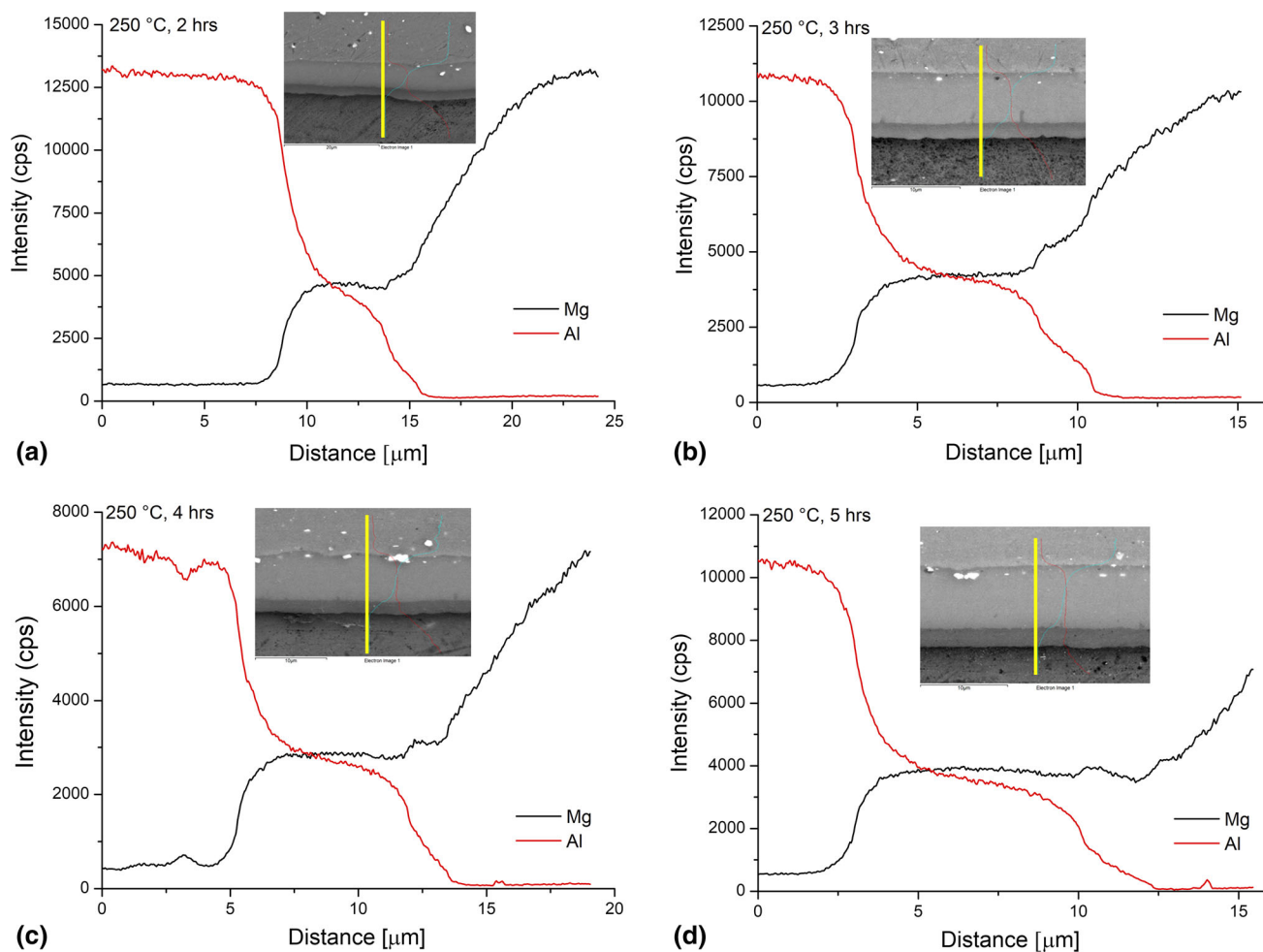


**Fig. 12** EDS linescan of Al and Mg through bimetal interface after annealing at 250  $^{\circ}C$  for (a) 2; (b) 3; (c) 4 and (d) 5 h (Color figure online)



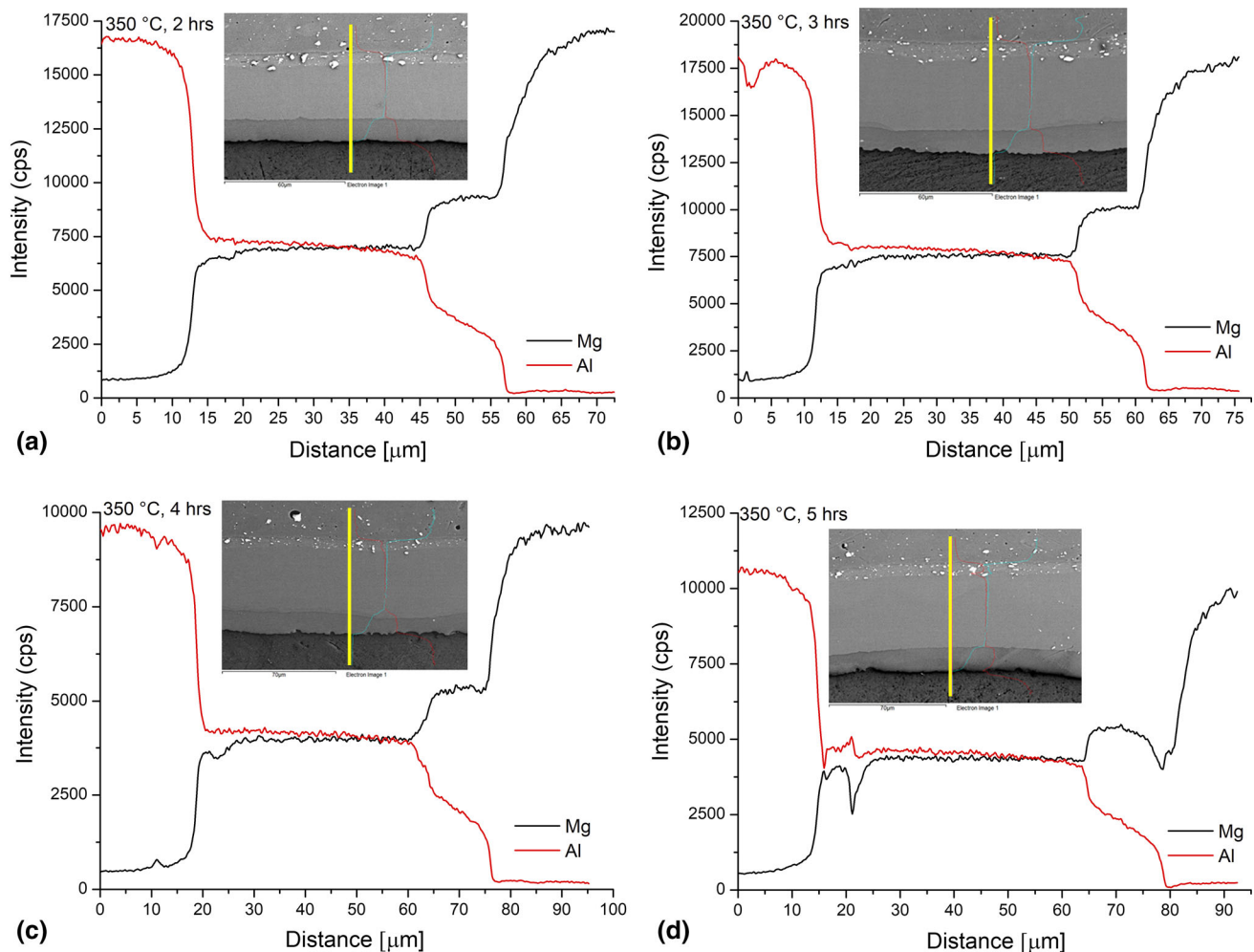


**Fig. 13** EDS linescan of Al and Mg through bimetal interface after annealing at 350 °C for (a) 2; (b) 3; (c) 4 and (d) 5 h (Color figure online)

different IMC layers were observed at the interface after annealing process. Based on obtained elemental linescans, it is visible that with the increase in the annealing temperature and time the thickness of IMC increases.

Elemental mapping of aluminum and magnesium is shown in Fig. 14(a), (b), (c), (d), (e), (f), (g), (h), and (i). Bimetal was annealed at 250, 300 and 350 °C for 5 h. Magnesium and aluminum are uniformly distributed at individual materials and the IMC layers as well. The brightest shade corresponds to the highest amount of investigated element. In the case of aluminum, the highest content is apparent in the upper sheet, i.e., AW5754 aluminum alloy. Darker shade is present nearby the AW5754 sheet, confirming the presence of  $Al_3Mg_2$ . The darkest shade of green color (aluminum) is present at the location close to the magnesium alloy ( $Mg_{17}Al_{12}$ ). Similar results were observed in the case of magnesium (red colored), but in the direction from AZ31B alloy toward interface. Some black spots (corresponding to bright particles rich in iron) were observed at the zone nearby AW5754 aluminum alloy. From Fig. 14, it is obvious that the increased temperature resulted in thickening of the IMC layers at the interface.

EDS point analysis was carried out to characterize the IMC interfacial layers. EDS analysis was carried out in Spectra 1 to 5 (bimetal annealed at 250 °C for 3 h) (Fig. 15a). The results of point analysis carried out in bimetal annealed at 250 °C for 3 h

are given in Table 3. The highest amount of aluminum (95.84 at.%) was detected in Spectrum 1. Furthermore, magnesium was detected in that location confirming the presence of 5000 series aluminum alloy. A decrease in aluminum content to about 62 at.% was recorded in Spectrum 2. An increase in magnesium was observed in that location (36.7 at.%). Further decrease in aluminum was measured in Spectrum 3. On the contrary, the increase in magnesium content was recorded. High content of magnesium confirming the presence of AZ31B magnesium alloy was detected in Spectrum 4. Furthermore, 3.36 at.% of aluminum and 0.48 at.% of zinc were detected. In Spectrum 5, the high amount of aluminum was detected. In this location, the highest content of iron was observed. The presence of element with higher atomic number was confirmed due to higher brightness of particle in Spectrum 5.

EDS analysis was further carried out in bimetal annealed at 250 °C for 5 (Spectra 1 to 5) (Fig. 15b). The results of point analysis carried out in bimetal after annealing at 250 °C for 5 h are specified in Table 4. Aluminum content of about 96.4 at.% and magnesium content of 3.4 at.% were recorded in Spectrum 1. Spectrum 2 (bright particle) was characterized by a higher amount of iron. In that case, the content of iron is 6.6 at.%. Spectrum 3 was characteristic by lower content of aluminum (about 57 at.%) and higher content of magnesium (42.3 at.%) in comparison to the previous Spectra. Further increase in

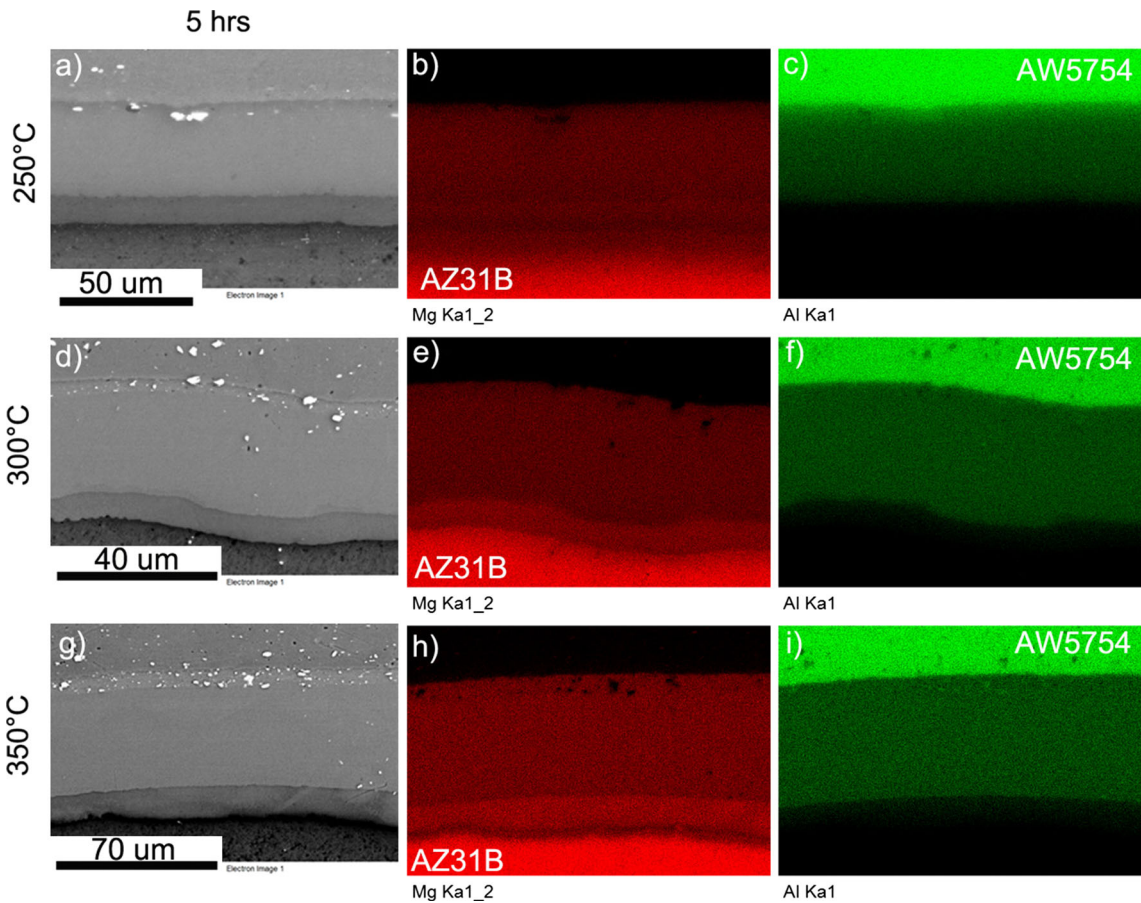


**Fig. 14** Elemental mapping across (a) bimetal interface after annealing at 250 °C for 5 h; with (b) magnesium distribution; (c) aluminum distribution; (d) bimetal interface after annealing at 300 °C for 5 h; with (e) magnesium distribution; (f) aluminum distribution; (g) bimetal interface after annealing at 350 °C for 5 h; with (h) magnesium distribution; (i) aluminum distribution

magnesium and decrease in aluminum content were observed in Spectrum 4. Spectrum 5 was characteristic by the highest amount of magnesium.

Locations of EDS analysis carried out in bimetal heat treated at 300 °C for 3 h (Spectra 1 to 4) are shown in Fig. 15c. High content of aluminum was recorded in Spectrum No. 1. Similarly, the occurrence of magnesium (about 4.1 at.%) was observed in that location. The content of aluminum 60 at.% and magnesium of 40 at.% was recorded in Spectrum No. 2. The presence of  $\text{Al}_3\text{Mg}_2$  IMC was confirmed based on the measured chemical composition. The content of magnesium of 61.5 at.% and aluminum of 37.5 at.% was detected in Spectrum 3, confirming the presence of  $\text{Mg}_{17}\text{Al}_{12}$  IMC. The content of magnesium of up to 96 at.% was observed in Spectrum No. 4.

Similar situation was observed in the bimetal after annealing at 300 °C for 5 h (Fig. 15d) and in bimetals annealed at 350 °C for 3 h (Fig. 15e) and for 5 h (Fig. 15f).

Results from EDS analysis and comparisons to aluminum-magnesium binary diagram proved that the layer close to the magnesium alloy consists of  $\text{Mg}_{17}\text{Al}_{12}$  IMC, and an area being close to aluminum alloy is formed by  $\text{Al}_3\text{Mg}_2$  IMC. Furthermore, the presence of particles with iron content was observed at the IMC–AW5754 interface. The diffusion of iron toward bimetal interface was confirmed. With the increase in annealing time, the content of iron was higher. Similarly, the increase in annealing temperature resulted in observation of particles with

increasing content of iron. These particles were spread in the dark matrix corresponding to the composition of  $\text{Al}_3\text{Mg}_2$ .

### 3.5 Measurements of Microhardness

The course of microhardness across as-welded bimetal interface is shown in Fig. 16(a). The increase in microhardness was recorded at the interface. Microhardness increase resulted from the work hardening induced by the high velocity impact. Furthermore, Loueiro et al. observed that the increase in explosive ratio resulted in increasing of the hardness of weld joints. It was associated with the faster impact of the flyer sheet (Ref 45).

The maximum microhardness in AZ31B side was measured 100 μm from the bimetal interface. The value was 106.4 HV0.025. AW5754 aluminum alloy microhardness increased toward the interface. The average microhardness of AW5754 was about 85 HV0.025. Microhardness increase in AZ31B was observed firstly 200 μm from the interface (91 HV0.025). At the distance of 100 μm, the value of 92 HV0.025 was measured. The microhardness increase is associated with the work hardening process. Aluminum alloys with the fcc lattice possess good ability to work harden. It is known that plastic deformation in aluminum at temperatures below 0.4 melting point is driven by the motion of lattice defects, i.e., dislocations. Thus, strain rate is coupled with the density of mobile dislocations and their mean velocity. Density of dislocations

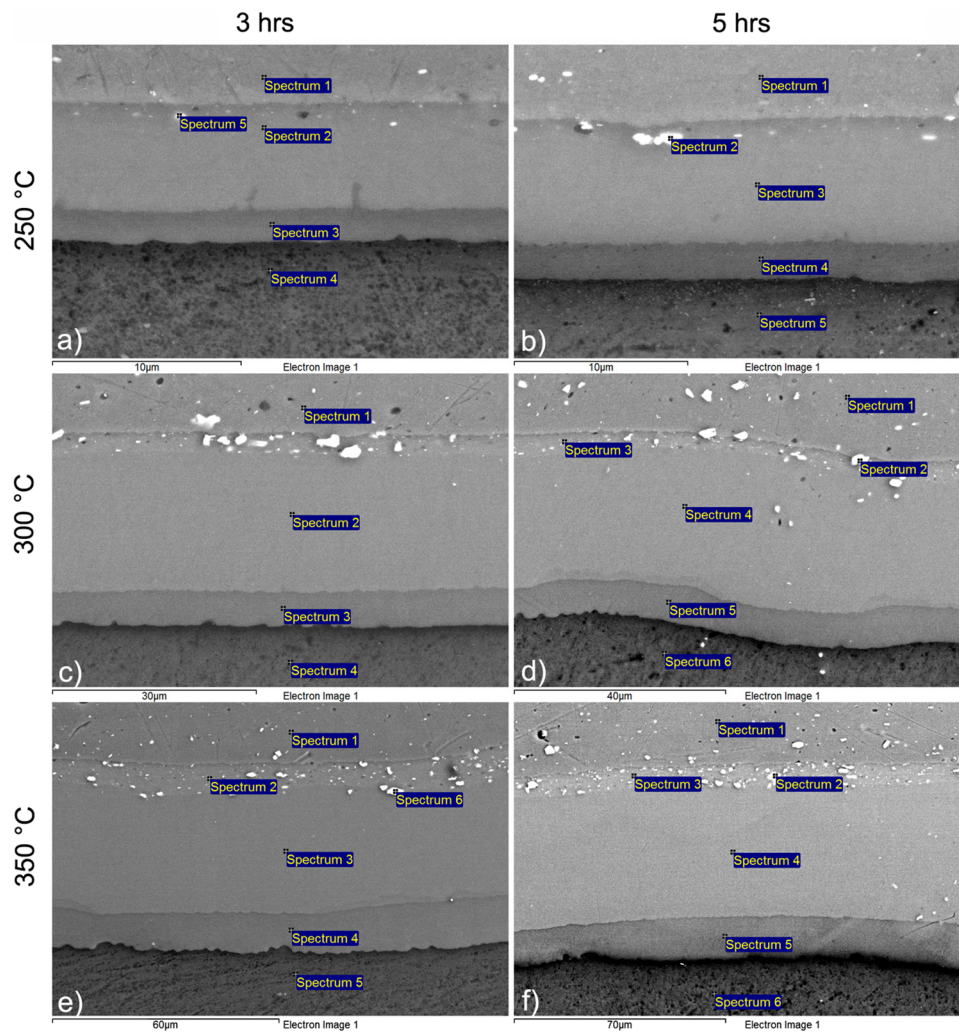


**Fig. 15** Point EDS analysis of bimetal interface annealed at 250 °C for (a) 3; (b) 5 h; annealed at 300 °C for (c) 3; (d) 5 h; annealed at 350 °C for (e) 3; (f) 5 h

**Table 3** EDS point analysis in bimetal after annealing at 250 °C for 3 h (in at.%)

Spectrum	Mg	Al	Si	Cr	Mn	Fe	Cu	Zn
1	4.06	95.84	...	...	0.10	...	...	...
2	36.68	62.51	...	...	0.14	0.07	...	0.60
3	63.08	35.06	...	...	0.15	...	0.11	1.61
4	96.07	3.36	0.09	...	...	...	...	0.48
5	25.00	68.29	1.10	0.24	1.63	3.50	...	0.25

**Table 4** EDS point analysis in bimetal after annealing at 250 °C for 5 h (in at.%)

Spectrum	Mg	Al	Si	Cr	Mn	Fe	Cu	Zn
1	3.40	96.36	...	0.04	0.10	...	0.10	...
2	20.05	68.18	2.07	0.12	2.86	6.60	0.11	...
3	42.27	57.12	0.05	...	...	...	...	0.56
4	70.10	27.57	0.12	...	0.13	...	...	2.07
5	95.55	3.66	0.20	...	0.18	...	...	0.41

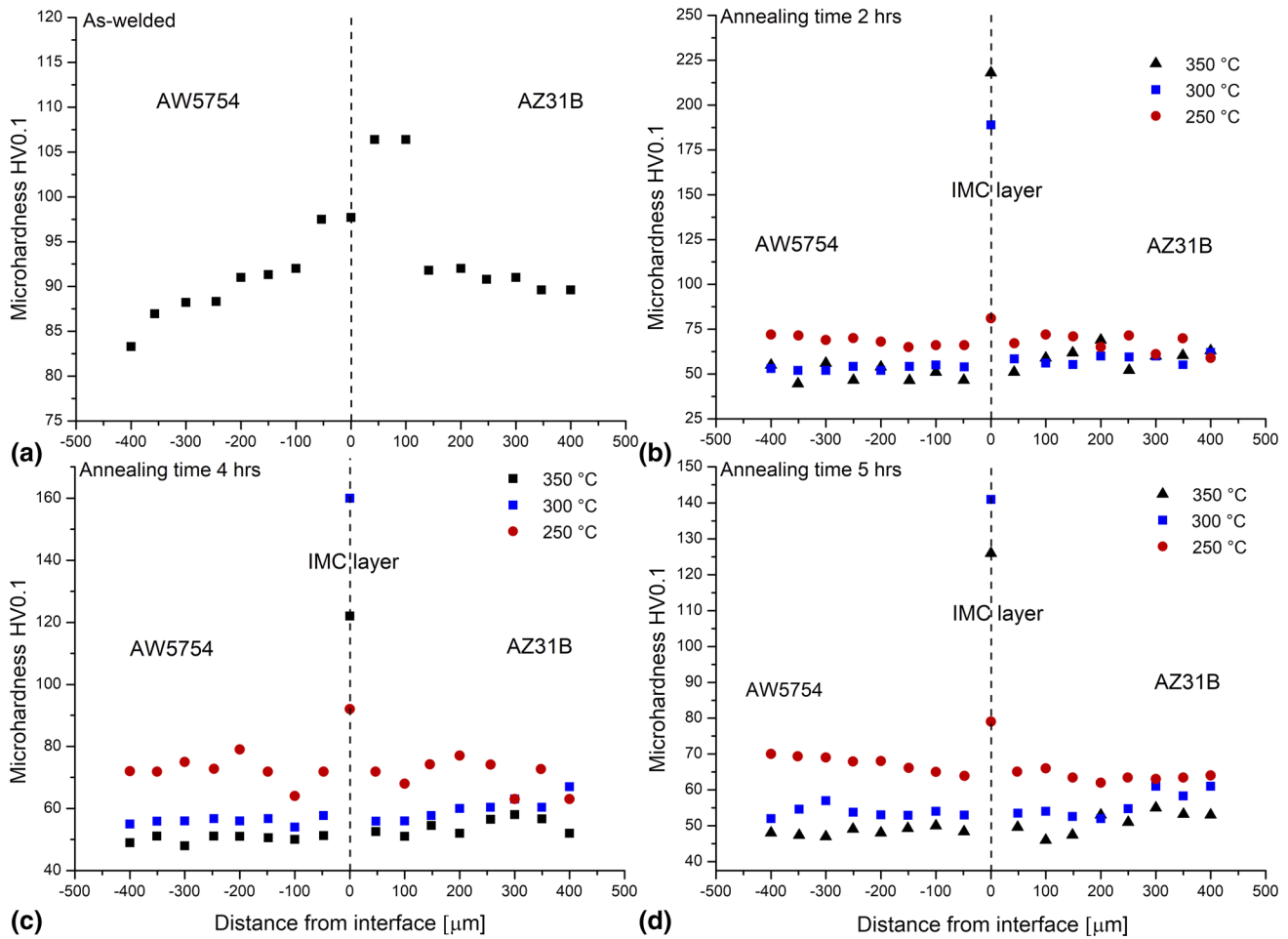


**Fig. 16** Course of microhardness across interface of (a) as-welded bimetal and after annealing at the temperatures of 250; 300 and 350 °C for (b) 2; (c) 4 and (d) 5 h

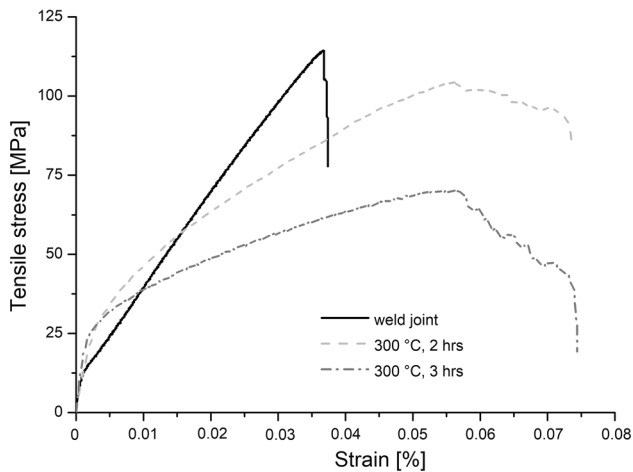


**Fig. 17** Stress vs. strain curves for as-welded and as-annealed AW5754-AZ31B bimetal

increases during deformation process (explosive welding in our case) and the stress for continuing the deformation rises as a result of the interaction of the mobile dislocations and network of dislocations present in material because of deformation (Ref 62).

The courses of microhardness across bimetal after annealing at 250, 300 and 350 °C for 2, 4 and 5 h are shown in Fig. 16(b), (c), and (d). The microhardness increased after annealing dramatically due to the occurrence of highly hard and brittle IMCs. Maximum microhardness values were measured in that location. The measured value is 218 HV0.025 for bimetal annealed at 350 °C for 2 h. By contrast, the mean microhardness decrease was observed in the flyer and the base metal, which relates to the process of recrystallization. The heat acting on the previously deformed materials led to dislocation annihilation and thus decreased the overall microhardness. Furthermore, increasing temperature/holding time resulted in grain growth. The drop in average microhardness of AW5754 aluminum alloy to about 48 HV0.025 was observed after annealing. Similarly, the decrease in microhardness of AZ31B magnesium alloy to about 50 HV0.025 was recorded, confirming the softening after annealing.

Jafarian et al. observed maximum microhardness in the middle of aluminum alloy-magnesium alloy diffusion bonded joints. Maximum microhardness was 140 HV for 6061-T6/AZ31 weld joint and 155 HV for 6061-O/AZ31 weld joint. Welding time for production of joints was 90 min at the temperature of 440 °C (Ref 16). Yan et al. observed that adiabatic shear bands and formation of twins in AZ31B contributed to work hardening. Furthermore, the hardening effect was also enhanced by stress formation originating from

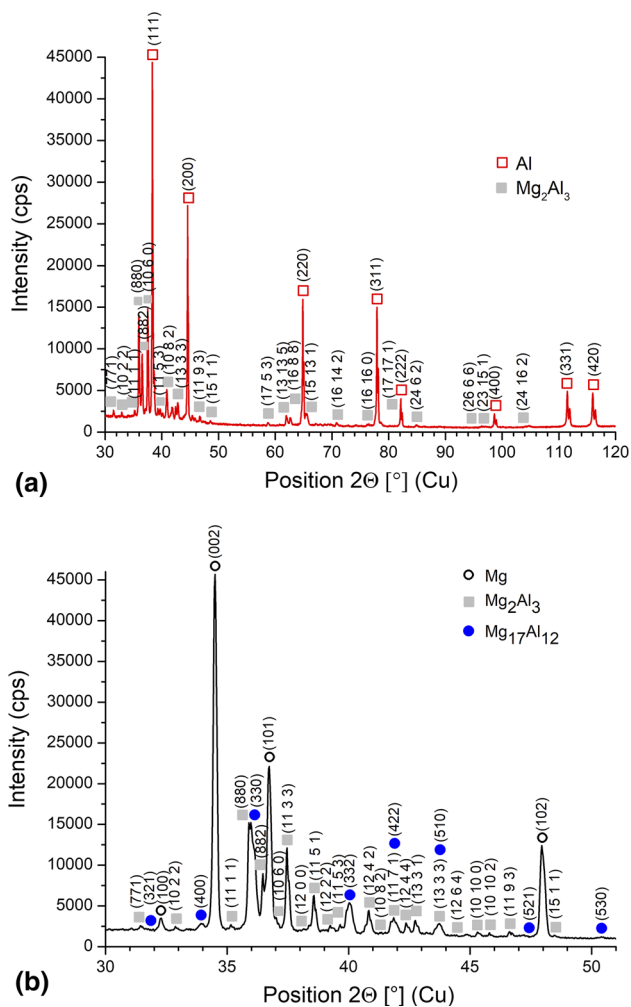


**Fig. 18** XRD patterns of fracture surfaces after tensile testing on (a) AW5754 flyer sheet side; (b) AZ31B base metal

different coefficients of thermal expansion for 7075 and AZ31B light alloys (Ref 8).

### 3.6 Tensile Strength of Bimetals

Stress–strain dependence of as-welded and as-annealed bimetal is specified in Fig. 17. The course of stress looks different for as-welded bimetal in comparison to as-annealed ones. The highest tensile strength is characteristic for bimetal as welded. The tensile strength averaged 120 MPa. No macroscopic delamination of the weld joint interface was observed. A drop in the tensile strength of bimetal annealed at 300 °C for 2 h was recorded. The tensile strength decreased to 104 MPa. This results from the formation of hard and brittle IMC after annealing. Zhang et al. (Ref 18) found the tensile strength of bimetal decreased significantly when the annealing temperature was equal to or above 250 °C.

The increasing of annealing time to 3 h resulted in thickening the interfacial IMC that resulted in further drop in tensile strength. Tensile strength reached 70 MPa in such a case.

Based on the results of tensile stress versus engineering strain dependence for AW5754-AZ31B dissimilar metals

bimetal, a sharp decrease in loading was observed after reaching the maximum strength. A few turns were obvious from the dependence for as-annealed bimetal. At this stage, delamination of the upper AW5754 aluminum sheet occurred. The maximum value in such a case corresponds to the state when delamination in the middle of specimen was observed (without fracturing base and flyer plate, as well). The interface was much more brittle in comparison with the base materials. The plastic properties of the IMC layer at the interface were too low. On the contrary, Zhang et al. (Ref 18) observed after delamination also fracturing both base and flyer plate. Jiaqi et al. firstly observed during tensile testing of magnesium alloy-titanium bimetal the fracture of AZ31B magnesium alloy. The fracture of TA2 titanium was observed later due to higher strength of titanium in comparison to that of magnesium alloy (Ref 51). Guo et al. analyzed dissimilar 7A04 aluminum alloy-AZ31 magnesium alloy inertia friction welds. The authors found that the weld with highest tensile strength  $R_m = 96$  MPa was produced when the friction pressure  $p = 124$  MPa was applied. Furthermore, all welds were fractured at the IMC layer-aluminum alloy interface. Quasi-cleavage fracture was observed in their study (Ref 63).

### 3.7 XRD Analysis of Fractured Surfaces

Qualitative phase analysis at the fractured surfaces after tensile testing of bimetal was performed by XRD. XRD patterns of fractured surfaces on both aluminum and magnesium alloy side after delamination of bimetal after annealing at 300 °C for 3 h are documented in Fig. 18(a), and (b).

The significant peaks of both aluminum (ICDD 00-004-0787) and  $Mg_2Al_3$  (ICDD 00-029-0048) IMC were detected at the aluminum sheet side (Fig. 16a). The highest intensity peak corresponding to Al was detected at the Bragg's angle  $2\Theta = 38.473^\circ$  from the plane (111). Aluminum is characterized by cubic crystal system, space group  $Fm\bar{3}m$  with space group number of 225. Lattice parameters are as follows:  $a = b = c = 4.0494$  Å and  $\alpha = \beta = \gamma = 90^\circ$ .

The highest intensity peak corresponding to  $Mg_2Al_3$  was detected at the Bragg's angle  $2\Theta = 37.523^\circ$  from the plane (1133).  $Mg_2Al_3$  is characterized by cubic crystal system, space group  $Fm\bar{3}m$ . Lattice parameters are as follows:  $a = b = c = 28.2390$  Å and  $\alpha = \beta = \gamma = 90^\circ$ . Significant peaks of magnesium (ICDD 00-004-0770),  $Mg_2Al_3$  (ICDD 00-029-0048) and  $Mg_{17}Al_{12}$  (ICDD 00-001-1128) IMCs were recorded at the magnesium sheet side (Fig. 6b). The highest intensity peak corresponding to magnesium was detected at the Bragg's angle  $2\Theta = 36.604^\circ$  from the plane (101). Magnesium is characterized by hexagonal crystal system, space group  $P63/mmc$ . Lattice parameters are as follows:  $a = b = 3.2095$  Å,  $c = 5.2104$ ,  $\alpha = \beta = 90^\circ$  and  $\gamma = 120^\circ$ . The highest intensity peak corresponding to  $Mg_2Al_3$  on the magnesium sheet side was detected at the Bragg's angle  $2\Theta = 37.523^\circ$  from the plane (1133). Furthermore, peaks of  $Mg_{17}Al_{12}$  IMC were recorded. The highest intensity peak corresponding to  $Mg_{17}Al_{12}$  on the magnesium sheet side was detected at the Bragg's angle  $2\Theta = 36.191^\circ$  from the plane (330).  $Mg_{17}Al_{12}$  is characterized by cubic crystal system, space group  $I\bar{4}3m$ . Lattice parameters are as follows:  $a = b = c = 10.56$  Å and  $\alpha = \beta = \gamma = 90^\circ$ .

IMCs were detected on both sides of fractured surfaces confirming that the IMCs degrade the mechanical properties of bimetal (Ref 63).

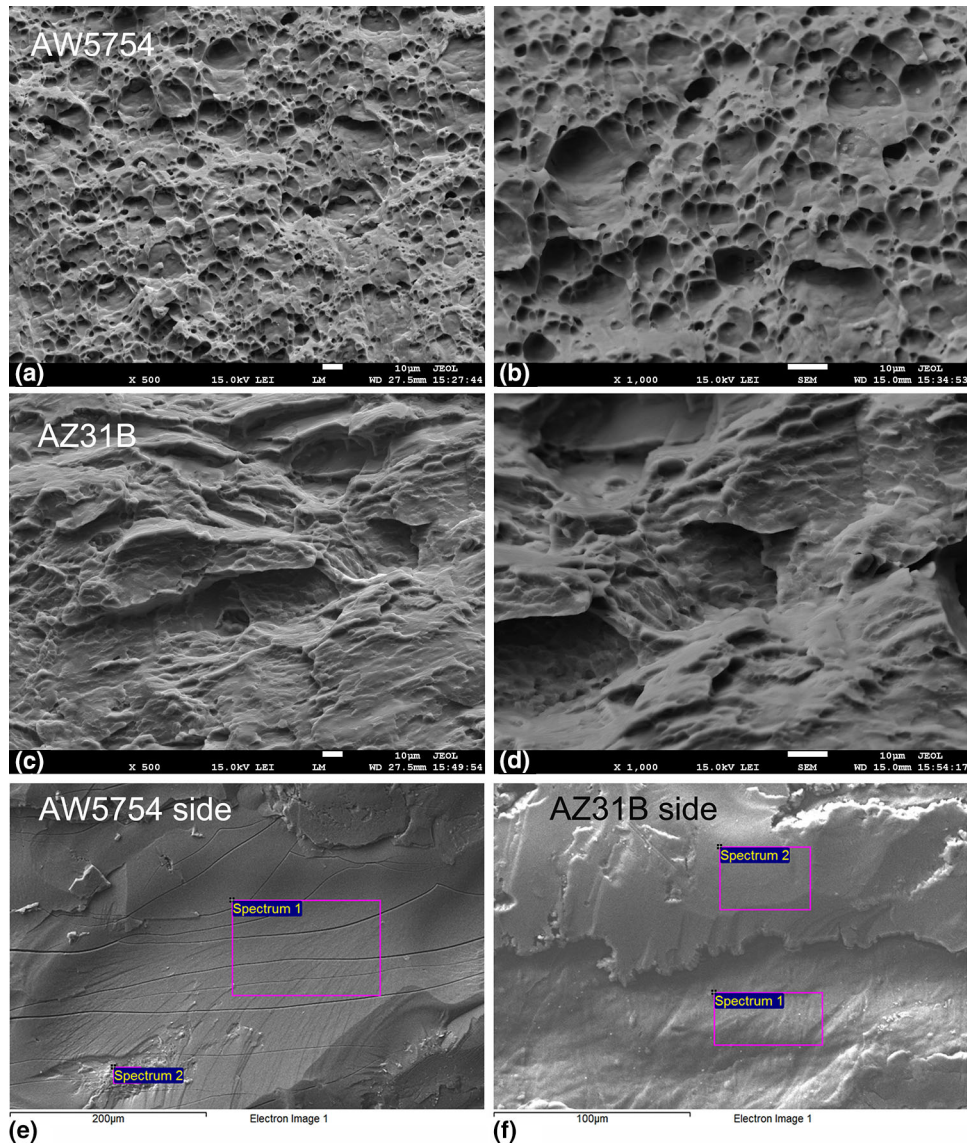


**Fig. 19** Fracture surfaces of bimetal after explosive welding on (a) AW5754 flyer with (b) detailed view; on (c) AZ31B alloy with (d) detailed view; fracture surfaces after annealing process on (e) AW5754 aluminum side and (f) AZ31B magnesium side

**Table 5** EDS point analysis on fracture surface of delaminated bimetal at AW5754 side (annealed at 300 °C for 3 h) (in at.%)

Spectrum	Mg	Al	Si	Cr	Mn	Fe	Cu	Zn
1	35.52	63.49	0.12	...	...	...	...	0.87
2	31.54	65.08	0.63	0.13	0.87	0.75	0.40	0.60

**Table 6** EDS point analysis on fracture surface of delaminated bimetal at AZ31B side (annealed at 300 °C for 3 h) (in at.%)

Spectrum	Mg	Al	Si	Zn
1	93.86	5.32	0.27	0.55
2	38.88	60.85	...	0.26

Similarly, Kimura et al. performed post weld heat treatment of aluminum-magnesium joint produced with friction welding. Heat treatment temperature of 400 °C and holding time of 24 h were used. Authors found that mainly  $Mg_{17}Al_{12}$  and  $Mg_2Al_3$  diffraction patterns and Al and Mg were found on the fracture surface of magnesium side. In addition, mainly  $Mg_{17}Al_{12}$  and  $Mg_2Al_3$  diffraction patterns and Al were recorded on the fracture surface of aluminum side (Ref 64). During annealing, the IMC layers growth process occurs via atoms diffusion at elevated temperatures. Interface layers of higher thickness are sites for initiation and propagation of cracking, which results in the decrease in interface strength. Authors observed columnar growth only in  $Mg_{17}Al_{12}$  layer in the welds annealed at 300 °C for 60 min (Ref 65). Jafarian et al. observed that x-ray diffraction patterns confirmed the creation of  $Mg_2Al_3$  and  $Al_{12}Mg_{17}$  IMCs in the interfacial zone. Authors observed the occurrence of the fracture in the location of IMCs being high hard and brittle (Ref 16).

### 3.8 Analysis of the Fracture Surfaces

Figure 19(a), (b), (c), and (d) shows the SEM image of fracture surfaces of bimetal in as-welded condition. Fracture surface of AW5754 (Fig. 19a, and b) after explosive welding is characteristic by the presence of dense network of dimples indicating the ductile fracture. In the AZ31B magnesium alloy fracture surfaces (Fig. 19c, and d), both dimples and cleavage planes were observed after explosive welding.

Fracture of as-welded bimetal propagated across the whole thickness of produced bimetal at the angle of approximately 45° to loading direction.

Mixed fracture consisting of ductile and brittle features is characteristic for lower part of produced bimetal. A similar situation was observed by Chen et al. (Ref 46).

Fracture surfaces of bimetal after annealing at 300 °C for 3 h are shown in Fig. 19(e), and (f). During tensile testing, the area with the presence of hard and brittle IMC cracked due to very low plasticity of the mentioned zone. Many cracks were found on the fracture surface on AW5754 aluminum alloy side confirming brittleness of mentioned zone. Delamination of upper sheet was observed during tensile testing of as-annealed specimens. Interface cracked in the layer consisting of Al<sub>3</sub>Mg<sub>2</sub>. The results of EDS point analysis on AW5754 aluminum side are given in Table 5. Spectra 1 and 2 (Table 5) are characteristic by the aluminum content of 31.5 to 35.5 at.% and aluminum content of 63.5 to 65 at.%. Brittle fracture was observed also on the AZ31B magnesium side (Table 6). Spectrum 2 corresponds to the composition of Al<sub>3</sub>Mg<sub>2</sub> IMC. In Spectrum 1, the IMC layer is completely debonded while revealing the surface of AZ31B magnesium alloy (content of about 94 at.% of magnesium).

## 4. Conclusion

The following can be concluded according to the results attained after analysis of the microstructure and mechanical properties of bimetals:

- AW5754 aluminum alloy-AZ31B magnesium alloy composite plate was characteristic by regular and wavy interface confirming the high quality of light alloys weld joint. The average length of waves was  $1218 \pm 48 \mu\text{m}$ , and amplitude of waves was  $276 \pm 11 \mu\text{m}$ .
- The increase in the thickness of IMC interfacial layer was observed with increasing of annealing temperature and time. IMC layer of highest thickness was recorded after annealing at 350 °C for 5 h and averaged 67  $\mu\text{m}$ .
- Both EDS and XRD analyses detected interfacial Mg<sub>17</sub>Al<sub>12</sub> and Al<sub>3</sub>Mg<sub>2</sub> IMCs after annealing of bimetals.
- Bright particles characteristic by higher amount of iron were distributed at the AW5754-Al<sub>3</sub>Mg<sub>2</sub> IMC interface.
- Rise in the microhardness at the interface of produced bimetal was associated with work hardening. Microhardness values increased to 218 HV0.025 after annealing process due to IMCs present at the interface.
- Tensile strength of AW5754-AZ31B bimetal in as-welded condition reached 120 MPa. Contrarily, the annealing process resulted in a decrease in bimetals tensile strength.

## Acknowledgments

The study was prepared under the support of the Project No. 1/1010/16 (VEGA grant agency of the Ministry of Education, Science, Research and Sport of the Slovak Republic and the Slovak Academy of Sciences). The paper is also the result of the project realization: CE for development and application of advanced diagnostic methods in processing of metallic and non-metallic materials—APRODIMET, ITMS:26220120048, supported by the Research & Development Operational Program funded by the ERDF.

## References

1. X. Fei, X. Jin, Y. Ye, T. Xiu, and H. Yang, Effect of Pre-hole Offset on the Property of the Joint During Laser-Assisted Friction Stir Welding of Dissimilar Metals Steel and Aluminum Alloys, *Mater. Sci. Eng., A*, 2016, **653**, p 43–52
2. W.J. Joost and P.J. Krajewski, Towards Magnesium Alloys for High-Volume Automotive Applications, *Scr. Mater.*, 2017, **128**, p 107–112
3. M. Vigaruddin and D.R. Reddy, Structural Optimization of Control Arm for Weight Reduction and Improved Performance, *Mater. Today Proc.*, 2017, **4**, p 9230–9236
4. B. Liu, A. Vivek, and G.S. Daehn, Joining Sheet Aluminum AA6061-T4 to Cast Magnesium AM60B by Vaporizing Foil Actuator Welding: Input Energy, Interface, and Strength, *J. Manuf. Process*, 2017, **30**, p 75–82
5. S. Chen and X. Jiang, Microstructure Evolution During Magnetic Pulse Welding of Dissimilar Aluminium and Magnesium Alloys, *J. Manuf. Process*, 2015, **19**, p 14–21
6. J. Teng, X. Gong, Y. Li, and Y. Nie, Influence of Aging on Twin Boundary Strengthening in Magnesium Alloys, *Mater. Sci. Eng., A*, 2018, **715**, p 137–143
7. S. You, Y. Huang, K.U. Kainer, and N. Hort, Recent Research and Developments on wrought Magnesium Alloys, *J. Magnes. Alloys*, 2017, **5**, p 239–253
8. Y.B. Yan, Z.W. Zhang, W. Shen, J.H. Wang, L.K. Zhang, and B.A. Chin, Microstructure and Properties of Magnesium AZ31B-Aluminum 7075 Explosively Welded Composite Plate, *Mater. Sci. Eng., A*, 2010, **527**, p 2241–2245
9. D.M. Fronczek, R. Chulist, L. Litynska-Dobrzynska, S. Kac, N. Schell, Z. Kania, Z. Szulca, and J. Wojewoda-Budka, Microstructure and Kinetics of Intermetallic Phase Growth of Three-Layered A1050/AZ31/A1050 Clads Prepared by Explosive Welding Combined with Subsequent Annealing, *Mater. Des.*, 2017, **130**, p 120–130
10. G. Casalino, P. Guglielmi, V.D. Lorusso, M. Mortello, P. Peyre, and D. Sorgente, Laser Offset Welding of AZ31B Magnesium Alloy to 316 Stainless Steel, *J. Mater. Process. Technol.*, 2017, **242**, p 49–59
11. L. Anicai, R. Masi, M. Santamaria, and F. Di Quatro, A Photoelectrochemical Investigation of Conversion Coatings on Mg Substrates, *Corros. Sci.*, 2005, **47**, p 2883–2900
12. H.Y. Hsiao and W.T. Tsai, Characterization of Anodic Films Formed on AZ91D Magnesium Alloy, *Surf. Coat. Technol.*, 2005, **190**, p 299–308
13. K.Z. Chong and T.S. Shih, Conversion-Coating Treatment for Magnesium Alloys by a Permanganate-Phosphate Solution, *Mater. Chem. Phys.*, 2003, **80**, p 191–200
14. F. Liu, W. Liang, X. Li, X. Zhao, Y. Zhang, and H. Wang, Improvement of Corrosion Resistance of Pure Magnesium Via Vacuum Pack Treatment, *J. Alloys Compd.*, 2008, **461**, p 399–403
15. Z. Liang, G. Qin, P. Geng, F. Yang, and X. Meng, Continuous drive Friction Welding of 5A33 Al Alloy to AZ31B Mg Alloy, *J. Manuf. Proc.*, 2017, **25**, p 153–162
16. M. Jafarian, M.S. Rizi, M. Jafarian, M. Honarmand, H.R. Javadinejad, A. Ghaheri, M.T. Bahramipour, and M. Ebrahimi, Effect of Thermal Tempering on Microstructure and Mechanical Properties of Mg-AZ31/Al-6061 Diffusion Bonding, *Mater. Sci. Eng., A*, 2016, **666**, p 372–379
17. F. Findik, Recent Developments in Explosion Welding, *Mater. Des.*, 2011, **32**, p 1081–1093

18. N. Zhang, W. Wang, X. Cao, and J. Wu, The Effect of Annealing on the Interface Microstructure and Mechanical Characteristics of AZ31B/AA6061 Composite Plates Fabricated by Explosive Welding, *Mater. Des.*, 2015, **65**, p 1100–1109
19. K.S. Lee, J.S. Kim, Y.M. Jo, S.E. Lee, J. Heo, Y.W. Chang, and Y.S. Lee, Interface-Related Deformation Behaviour of a Stainless Steel-Al-Mg 3-ply Composite, *Mater. Charact.*, 2013, **75**, p 138–149
20. X.P. Zhang, T.H. Yang, S. Castagne, and J.T. Wang, Microstructure; Bonding Strength and Thickness Ratio of Al/Mg/Al Alloy Laminated Composites Prepared by Hot Rolling, *Mater. Sci. Eng., A*, 2011, **528**, p 1954–1960
21. K.S. Lee, D.H. Yoon, H.K. Kim, Y.N. Kwon, and Y.S. Lee, Effect of Annealing on the Interface Microstructure and Mechanical Properties of a STS-Al-Mg 3-ply Clad Sheet, *Mater. Sci. Eng., A*, 2012, **556**, p 319–330
22. P. Liu, Y. Li, H. Geng, and J. Wang, Microstructure Characteristics in TIG Welded Joint of Mg/Al Dissimilar Materials, *Mater. Lett.*, 2007, **61**, p 1288–1291
23. R. Borrisutthekul, Y. Miyashita, and Y. Mutoh, Dissimilar Material Laser Welding Between Magnesium Alloy AZ31B and Aluminium Alloy A5052-O, *Sci. Technol. Adv. Mater.*, 2005, **6**, p 199–204
24. L.M. Liu, H.Y. Wang, and Z.D. Zhang, The Analysis of Laser Weld Bonding of Al Alloy to Mg Alloy, *Scr. Mater.*, 2007, **56**, p 473–476
25. R. Cao, B.F. Wen, J.H. Chen, and PCh Wang, Cold Metal Transfer Joining of Magnesium AZ31B-to-Aluminum A6061-T6, *Mater. Sci. Eng., A*, 2013, **560**, p 256–266
26. J. Shang, K. Wang, Q. Zhou, D. Zhang, J. Huang, and G. Li, Microstructure Characteristics and Mechanical Properties of Cold Metal Transfer Welding Mg/Al Dissimilar Metals, *Mater. Des.*, 2012, **34**, p 559–565
27. J. Shang, K. Wang, Q. Zhou, D. Zhang, J. Huang, and G. Li, Microstructure Characteristics and Properties of Mg/Al Dissimilar Metals made by Cold Metal Transfer Welding with ER4043 Filler Metal, *Rare Met. Mater. Eng.*, 2013, **42**, p 1337–1341
28. M. Sun, S.T. Niknejad, H. Gao, L. Wu, and Y. Zhou, Mechanical Properties of Dissimilar Resistance Spot Welds of Aluminum to Magnesium with Sn-Coated Steel Interlayer, *Mater. Des.*, 2016, **91**, p 331–339
29. M. Sun, S.T. Niknejad, G. Zhang, M.K. Lee, L. Wu, and Y. Zhou, Microstructure and Mechanical Properties of Resistance Spot Welded AZ31/AA5754 Using a Nickel Interlayer, *Mater. Des.*, 2015, **87**, p 905–913
30. T. Yang, K. Wang, D. Zhang, and J. Huang, Contact-Reaction Brazing of an AZ31 Magnesium/3003 Aluminum Alloy Using a Silver-Copper-Zinc Interlayer, *J. Mater. Process. Technol.*, 2017, **249**, p 531–537
31. Z. Wang, H. Wang, and L. Liu, Study on Low Temperature Brazing of Magnesium Alloy to Aluminum Alloy Using Sn-xZn Solders, *Mater. Des.*, 2012, **39**, p 14–19
32. M. Jafarian, A. Khodabandeh, and S. Manafi, Evaluation of Diffusion Welding of 6061 Aluminum and AZ31 Magnesium Alloys Without Using an Interlayer, *Mater. Des.*, 2015, **65**, p 160–164
33. S.S. Seyyed Afghahi, M. Jafarian, M. Paidar, and M. Jafarian, Diffusion Bonding of Al 7075 and Mg AZ31 Alloys: Process Parameters, Microstructural Analysis and Mechanical Properties, *Trans. Nonferrous Met. Soc. China*, 2016, **26**, p 1843–1851
34. W. Liu, L. Long, Y. Ma, and L. Wu, Microstructure Evolution and Mechanical Properties of Mg/Al Diffusion Bonded Joints, *J. Alloys Compd.*, 2015, **643**, p 34–39
35. Y. Li, P. Liu, J. Wang, and H. Ma, XRD and SEM Analysis Near the Diffusion Bonding Interface of Mg/Al Dissimilar Materials, *Vacuum*, 2007, **82**, p 15–19
36. A. Azizi and H. Alimardan, Effect of Welding Temperature and Duration on Properties of 7075 Al to AZ31B Mg Diffusion Bonded Joint, *Trans. Nonferrous Met. Soc. China*, 2016, **26**, p 85–92
37. J. Zhang, G. Luo, Y. Wang, Q. Shen, and L. Zhang, An Investigation on Diffusion Bonding of Aluminum and Magnesium Using a Ni Interlayer, *Mater. Lett.*, 2012, **83**, p 189–191
38. V. Paradiso, F. Rubino, P. Carlone, and G.S. Palazzo, Magnesium and Aluminium Alloys Dissimilar Joining by Friction Stir Welding, *Procedia Eng.*, 2017, **183**, p 239–244
39. B. Fu, G. Qin, F. Li, X. Meng, and Ch Wu, Friction Stir Welding Process of Dissimilar Metals of 6061-T6 Aluminum Alloy to AZ31B Magnesium Alloy, *J. Mater. Process. Technol.*, 2015, **218**, p 38–47
40. R.K. Jayraj, S. Malarvizhi, and V. Balasubramanian, Electrochemical Corrosion Behavior of Stir Zone of Friction Stir Welded Dissimilar Joints of AA6061 Aluminium-AZ31B Magnesium Alloys, *Trans. Nonferrous Met. Soc. China*, 2017, **27**, p 2181–2192
41. Y. Zhao, Z. Lu, K. Yan, and L. Huang, Microstructural Characterizations and Mechanical Properties in Underwater Friction Stir Welding of Aluminum and Magnesium Dissimilar Alloys, *Mater. Des.*, 2015, **65**, p 675–681
42. J. Mohammadi, Y. Behnamian, A. Mostafaei, H. Izadi, T. Saeid, A.H. Kokabi, and A.P. Gerlich, Friction Stir Welding Joint of Dissimilar Materials Between AZ31B Magnesium and 6061 Aluminum Alloys: Microstructure Studies and Mechanical Characterizations, *Mater. Charact.*, 2015, **101**, p 189–207
43. A. Macwan and D.L. Chen, Ultrasonic Spot Welding of Rare-Earth Containing ZEK100 Magnesium Alloy to 5754 Aluminum Alloy, *Mater. Sci. Eng., A*, 2016, **666**, p 139–148
44. T. Zhang, W. Wang, W. Zhang, Y. Wei, X. Cao, Z. Yan, and J. Zhou, Microstructure Evolution and Mechanical Properties of an AA6061/AZ31B Alloy Plate Fabricated by Explosive Welding, *J. Alloys Compd.*, 2018, **735**, p 1759–1768
45. A. Loureiro, R. Mendes, J.B. Ribeiro, R.M. Leal, and I. Galvão, Effect of Explosive Mixture on Quality of Explosive Welds of Copper to Aluminium, *Mater. Des.*, 2016, **95**, p 256–267
46. Zh Chen, D. Wang, X. Cao, W. Yang, and W. Wang, Influence of Multi-pass Rolling and Subsequent Annealing on the Interface Microstructure and Mechanical Properties of Explosive Welding Mg/Al Composite Plates, *Mater. Sci. Eng., A*, 2018, **723**, p 97–108
47. T. Zhang, W. Wang, W. Zhang, Y. Wei, X. Cao, Zh Yan, and J. Zhou, Microstructure Evolution and Mechanical Properties of an AA6061/AZ31B Alloy Plate Fabricated by Explosive Welding, *J. Alloys Compd.*, 2018, **735**, p 1759–1768
48. Y.-L. Ding, J.-G. Wang, M. Zhao, and D.-Y. Ju, Effect of Annealing Temperature on Joints of Diffusion Bonded Mg/Al Alloys, *Trans. Nonferrous Met. Soc. China*, 2018, **28**, p 251–258
49. Ch Luo, W. Liang, Zh Chen, J. Zhang, Ch Chi, and F. Yang, Effect of High Temperature Annealing and Subsequent Hot Rolling on Microstructural Evolution at the Bond Interface of Al/Mg/Al Alloy Laminated Composites, *Mater. Charact.*, 2013, **84**, p 34–40
50. A. Macwan, X.Q. Jiang, C. Li, and D.L. Chen, Effect of Annealing on Interface Microstructures and Tensile Properties of Rolled Al/Mg/Al Tri-Layer Clad Sheets, *Mater. Sci. Eng., A*, 2013, **587**, p 344–351
51. Wu Jiaqi, Wang Wenxian, Cao Xiaoping, and Zhang Nan, Interface Bonding Mechanism and Mechanical Behavior of AZ31B/TA2 Composite Plate Cladded by Explosive Welding, *Rare Met. Mater. Eng.*, 2017, **46**, p 0640–0645
52. P. Bazarnik, B. Adamczyk-Cieślak, A. Gałka, B. Płonka, L. Sniezek, M. Cantoni, and M. Lewandowska, Mechanical and Microstructural Characteristics of Ti6Al4V/AA2519 and Ti6Al4V/AA1050/AA2519 Laminates Manufactured by Explosive Welding, *Mater. Des.*, 2016, **111**, p 146–157
53. I.A. Bataev, A.A. Bataev, V.I. Mali, and D.V. Pavliukova, Structural and Mechanical Properties of Metallic-Intermetallic Laminate Composites Produced by Explosive Welding and Annealing, *Mater. Des.*, 2012, **35**, p 225–234
54. M. Sahul, M. Sahul, J. Lokaj, Ľ. Čaplovič, and P. Nesvadba, Influence of Annealing on the Properties of Explosively Welded Titanium Grade 1—AW7075 Aluminum Alloy Bimetals, *J. Mater. Eng. Perform.*, 2018, **27**, p 5665–5674
55. G.H.S.F.L. Carvalho, R. Mendes, R.M. Leal, I. Galvão, and A. Loureiro, Effect of the Flyer Material on the Interface Phenomena in Aluminium and Copper Explosive Welds, *Mater. Des.*, 2017, **122**, p 172–183
56. B.A. Greenberg, M.A. Ivanov, V.V. Rybin, O.A. Elkina, O.V. Antonova, A.M. Patselov, A.V. Inozemtsev, A.V. Plotnikov, AYU Volkova, and YuP Besshaposnikov, The Problem of Intermixing of Metals Possessing no Mutual Solubility Upon Explosion Welding (Cu-Ta, Fe-Ag, Al-Ta), *Mater. Charact.*, 2013, **75**, p 51–62
57. D.V. Lazurenko, I.A. Bataev, V.I. Mali, A.A. Bataev, IuN Maliutina, V.S. Lozhkin, M.A. Esikov, and A.M.J. Jorge, Explosively Welded Multilayer Ti-Al Composites: Structure and Transformation during Heat Treatment, *Mater. Des.*, 2016, **102**, p 122–130
58. I.A. Bataev, D.V. Lazurenko, S. Tanaka, K. Hokamoto, A.A. Bataev, Y. Guo, and A.M. Jorge, Jr., High Cooling Rates and Metastable Phases at



- the Interfaces Of Explosively Welded Materials, *Acta Mater.*, 2017, **135**, p 277–289
59. Y. Wang and PhB Prangnell, The Significance of Intermetallic Compounds Formed During Interdiffusion in Aluminium and Magnesium Dissimilar Welds, *Mater. Charact.*, 2017, **134**, p 84–95
  60. Y. Yang, F. Zhang, J. He, Y. Qin, B. Liu, M. Yang, and F. Yin, Microstructure, Growth Kinetics and Mechanical Properties of Interface Layer for Roll Bonded Aluminium-Steel Clad Sheet Annealed under Argon Gas Protection, *Vacuum*, 2018, **151**, p 189–196
  61. Z.F. Li, J. Dong, X.Q. Zheng, C. Lu, W.J. Ding, and Z.M. Ren, Influence of Strong Static Magnetic Field on Intermediate Phase Growth in Mg-Al Diffusion Couple, *J. Alloys Compd.*, 2007, **440**, p 132–136
  62. R. Lumey, *Fundamentals of Aluminium Metallurgy: Production, Processing and Applications*, Elsevier, Amsterdam, 2010, ISBN 9780857090256
  63. W. Guo, G. You, G. Yuan, and X. Zhang, Microstructure and Mechanical Properties of Dissimilar Inertia Friction Welding of 7A04 Aluminium Alloy to AZ31 Magnesium Alloy, *J. Alloys Compd.*, 2017, **695**, p 3267–3277
  64. M. Kimura, A. Fuji, and S. Shibata, Joint Properties of friction Welded Joint Between Pure Magnesium and Pure Aluminium with Post-weld Heat Treatment, *Mater. Des.*, 2015, **85**, p 169–179
  65. J.-S. Kim, K.-S. Lee, Y.-N. Kwon, B.-J. Lee, and Y.-W. Chang, Improvement in Interfacial Bonding Strength in Roll-Bonded Mg/Al Clad Sheets through Annealing and Secondary Rolling Process, *Mater. Sci. Eng., A*, 2015, **628**, p 1–10

**Publisher's Note** Springer Nature remains neutral with regard to jurisdictional claims in published maps and institutional affiliations.